CHALMERS
UNIVERSITY OF TECHNOLOGY

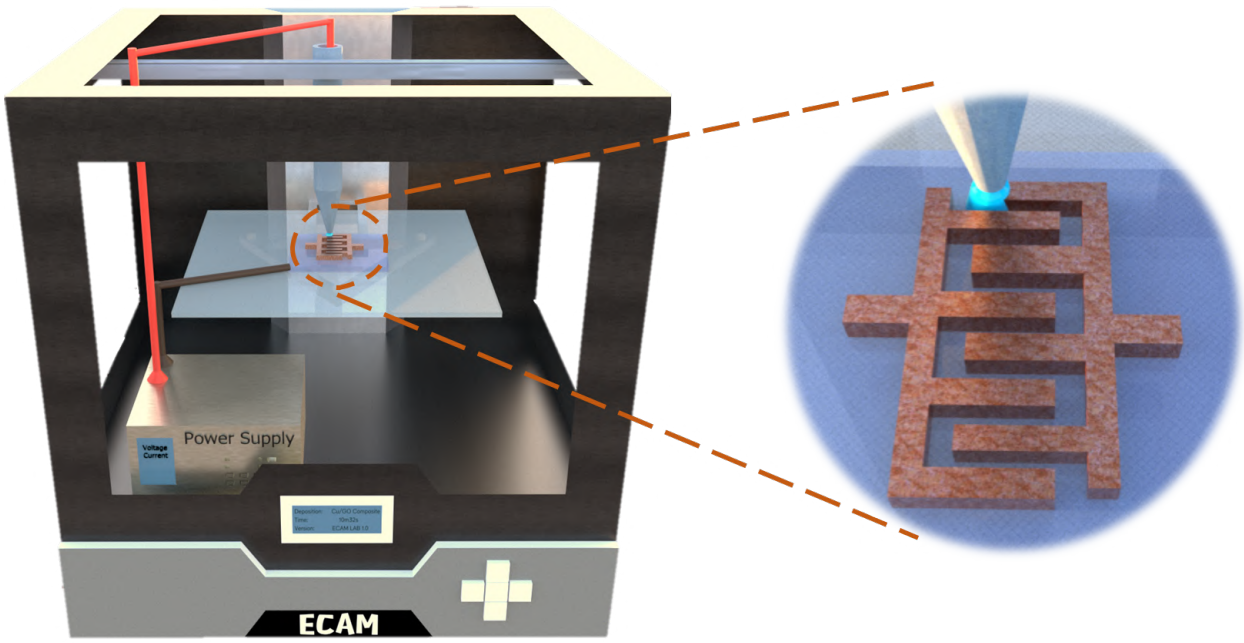

Electrochemical Micromanufacturing of Copper/Graphene Oxide Composites

An additive fabrication process with gel precursors

Master's thesis in Materials Engineering

KAITUO ZHANG

DEPARTMENT OF INDUSTRIAL AND MATERIALS SCIENCE

CHALMERS UNIVERSITY OF TECHNOLOGY
Gothenburg, Sweden 2023
www.chalmers.se

Master's thesis 2023

Electrochemical Micromanufacturing of Copper/Graphene Oxide Composites

An additive fabrication process with gel precursors

KAITUO ZHANG

CHALMERS
UNIVERSITY OF TECHNOLOGY

Department of Industrial and Materials Science
Division of Materials and Manufacture
Chalmers University of Technology
Gothenburg, Sweden 2023

Electrochemical Micromanufacturing of Copper/Graphene Oxide Composites
An additive fabrication process with gel precursors
KAITUO ZHANG

Supervisor: Zhenyuan Xia, Department of Industrial and Materials Science
Examiner: Uta Klement, Department of Industrial and Materials Science

Master's Thesis 2023
Department of Industrial and Materials Science
Division of Materials and Manufacture
SE-412 96 Gothenburg
Telephone +46 31 772 1000

Cover: Schematic diagram of modified desktop 3D printer for ECAM.

Typeset in LaTeX
Printed by Chalmers Reproservice
Gothenburg, Sweden 2023

Electrochemical Micromanufacturing of Copper/Graphene Oxide Composites
An additive fabrication process with gel precursors
KAITUO ZHANG
Department of Industrial and Materials Science
Division of Materials and Manufacture
Chalmers University of Technology

Abstract

Electrochemical Additive Manufacturing (ECAM) is a simple and efficient micro 3D metal manufacturing method that nowadays has great potential in various areas, especially in functional materials such as electrode materials. However, maintaining a steady water droplet connection between the printing nozzle and substrates is indeed a challenge in the current meniscus-confined ECAM technique. In order to better control the droplet formation for micro ECAM, to enhance the meniscus stability and to simplify the process, this work introduces cellulose based gels as novel precursors for ECAM to fabricate copper (Cu) on different substrates. In addition, different levels of Graphene Oxide (GO) were added to improve the structural and electrochemical properties of the deposits, i.e. corrosion resistance. The effects of GO in the Cu-based deposits were investigated in detail by Scanning Electron Microscopy (SEM), Raman Spectroscopy, X-ray Photo-electron Spectroscopy (XPS), Cyclic Voltammetry (CV) and corrosion tests, including surface morphology and composition analysis, as well as corrosion resistance in 3.5% $NaCl$ solution. Ultimately, gel-like precursors suitable for the micro ECAM process were successfully prepared. A series of samples with GO content of 0.1 - 3.0 $wt.\%$ of copper ions were then prepared on this basis, and in comparison with pure Cu samples, it was concluded that GO reduced the corrosion current density by 26.6% to 65.6%.

Keywords: electrochemical additive manufacturing, electrochemical deposition, gel precursors, 3D printing, graphene oxide, corrosion test.

Acknowledgements

They either gave me the opportunity to study at Chalmers, helped me immensely along this way, or inadvertently taught me more than just academics. The names below, including but not limited to them, are in alphabetical order.

Antonio Mulone	Atsuya Watanabe	Changjie Huang	Charlott Ågren
Didarul Alam	Eric Tam	Fang Liu	Hanli Bao
Haowei Liao	James Randall	Jessica Twedmark	Jiahao Shi
Jie Hao	Jinfeng Wu	Johan Malmqvist	Junmei Hao
Kaituo Zhang	Karthik Jayakumar	Keyvan Mirehbar	Nikhil Belsure
Pan Hu	Peter Hammersberg	Qian Zhang	Qiang Zhang
Qingde Zhang	Ren Wang	Roger Sagdahl	Ru Zhang
Ruiqi Chen	Sankar Sasidharan	Shanchao Bao	Shichao Hao
Shikai Hao	Side Zhang	Stefan Gustafsson	Tiance An
Tianlin Zhang	Tianyi Bao	Uta Klement	Xiaolong Li
Xiaoqi Liu	Xinhao Wang	Ya Wen	Yu Cao
Yunlin Ma	Zhaoyang Li	Zhenyuan Xia	All patrons

Thanks! Tack! Gǎn xiè!

Kaituo Zhang, Gothenburg, Jun 2023

List of Acronyms

2D Two-Dimensional
3D Three-Dimensional

Al Aluminium
AM Additive Manufacturing

BJT Binder Jetting
BTA Benzotriazole

C Carbon
CAD Computer Aided Design
CE Counter Electrode
CMC Carboxymethyl Cellulose
Cu Copper
CV Cyclic Voltammetry

DC Direct Current
DED Direct Energy Deposition
DMM Digital Multi Meter

ECAM Electrochemical Additive Manufacturing
ECD Electrochemical Deposition

FDM Fused Deposition Modelling

G-code Geometric Code
GO Graphene Oxide

HOPG Highly Oriented Pyrolytic Graphite

ITO Indium Tin Oxide

LPR Linear Polarisation Resistance

M.W. Molecular Weight
MC Methyl Cellulose

N Nitrogen
NaCl Sodium Chloride

O Oxygen

OM Optical Microscopy

PBF Powder Bed Fusion
PDDA Poly(diallyldimethylammonium chloride)
Pt Platinum
PVA Polyvinyl Alcohol

Raman Raman Spectroscopy
RE Reference Electrode
rGO reduced Graphene Oxide

SEK Swedish Krona
SEM Scanning Electron Microscopy
SHL Sheet Lamination
STL Standard Triangle Language

WE Working Electrode

XPS X-ray Photo-electron Spectroscopy

List of Symbols

$\boldsymbol{at.\%}$ atomic percent

$\boldsymbol{cm^{-1}}$ inverse centimeters
$\boldsymbol{cP}$ centipoise

$\boldsymbol{^{\circ}C}$ degree Celsius

$\boldsymbol{E_{corr}}$ corrosion potential
$\boldsymbol{eV}$ electron volt

$\boldsymbol{g/L}$ gram per litre

$\boldsymbol{i_{corr}}$ corrosion current density
$\boldsymbol{I_D}$ intensity of D band
$\boldsymbol{I_G}$ intensity of G band

$\boldsymbol{kV}$ kilo volt

$\boldsymbol{M}$ metal
$\boldsymbol{mA}$ milliampere
$\boldsymbol{mA/cm^2}$ milliamperes per square centimeters
$\boldsymbol{mL}$ millilitre
$\boldsymbol{mm}$ millimetre
$\boldsymbol{mmol/L}$ millimole per litre
$\boldsymbol{mm/s}$ millimetre per second
$\boldsymbol{mm^2}$ square millimetre
$\boldsymbol{mol/L}$ molar per litre
$\boldsymbol{\mu m}$ micrometre
$\boldsymbol{mV}$ millivolt
$\boldsymbol{mV/s}$ millivolt per second
$\boldsymbol{mW}$ milliwatt

$\boldsymbol{n}$ number of electrons
$\boldsymbol{nm}$ nanometre

$\boldsymbol{rpm}$ revolutions per minute

$\boldsymbol{V}$ volt

$\boldsymbol{W}$ watt
$\boldsymbol{wt.\%}$ percentage by mass

Contents

List of Figures

List of Tables

1 Introduction

1.1 Background

1.1.1 Metallic micro additive manufacturing (AM) techniques

Additive Manufacturing (AM), or Three-Dimensional (3D) printing, is a fabrication technique from a digital model, usually a Computer Aided Design (CAD) file, through the layer-by-layer deposition of materials to highly customised, more sustainable and high complex objects[1]. Right now, AM technology is widely used to fabricate metallic parts by Powder Bed Fusion (PBF), and Direct Energy Deposition (DED), Binder Jetting (BJT) and Sheet Lamination (SHL)[1, 2]. And laser, electron beam, arc and ultrasound are considered as energy source for joining raw materials, such as powder, wire and sheets[3]. In terms of micro production process for metallic AM, PBF is the most common way and has the highest resolution, around 50 microns to 200 microns[4]. The principle of PBF is formed of three steps, the movement of platform, the supplying of powder and the consolidate of powder[5], then the cycle of three steps brings the final parts, as described in Fig. 1.1.

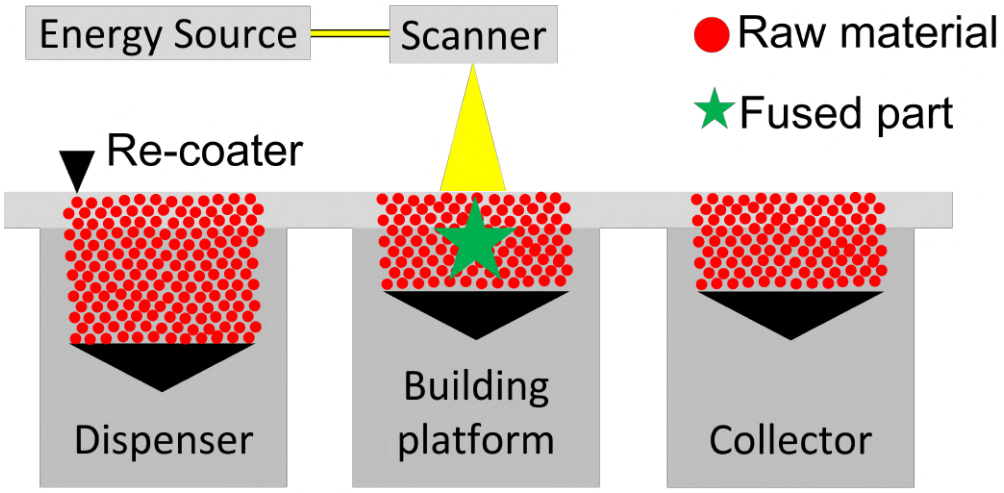

Figure 1.1: Schematic diagram of PBF

But there are still several aspects of additive manufacturing that could be improved, such as the relatively high machine costs[3, 4] and raw material cost[3, 6, 7], strict working environment requirements[7, 8] and limited choice of materials[5, 6, 9] compared to conventional metal processing technology. The PBF machine costs millions

of Swedish Krona (SEK), and virgin raw materials instead of recycled ones are normally needed for the best quality of final products. And vacuum or inert gas environment is a must for PBF process and high temperature is maintained throughout manufacturing. Materials developed for PBF include but are not limited to titanium, nickle, steel, aluminium and their alloys.

1.1.2 Electrochemical deposition (ECD)

Electrochemical Deposition (ECD), also known as electroplating and electrodeposition, is a method that metal cations are reduced by direct current to produce a metallic coating on a solid substrate. It thereby prevents metal oxidation, such as rust, improves wear resistance, electrical conductivity, reflective properties, corrosion resistance and enhances aesthetics. ECD requires less electrical power than other copper production methods such as smelting and refining, making it more cost-effective and energy-efficient. At the same time, almost no waste is produced in the process, only remaining electrolyte which can be easily disposed of. In general, ECD is an easy-to-operate, low-cost and well-developed technology.

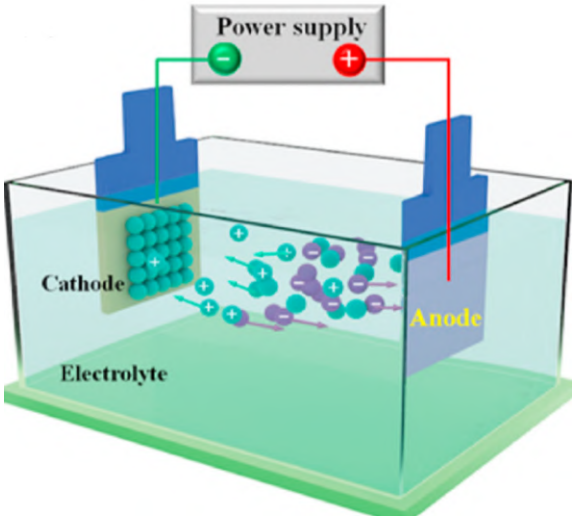

Figure 1.2: Schematic diagram of ECD. (Reproduced from Ref.[10] with permission from Elsevier)

1.1.3 Electrochemical additive manufacturing (ECAM)

Electrochemical Additive Manufacturing (ECAM), an emerging manufacture method that combines AM process and ECD[11], has been developed as an alternative to conventional metallic AM method. During the ECAM process, a localised ECD occurs on the target electrode surface with simultaneous migration and reduction of metal ions inside an electrolyte media. In contrast to the conventional ECD technique that usually deposits metallic compounds on a large area, ECAM allows precise deposition of metal-based materials on a flat substrate (cathode) within a confined micro-space. ECAM could also realise atomic-level deposition of various materials (i.e. metal and alloy components) with versatile deposition control param-

eters, which is a promising technique for room-temperature production of micro- and nano-scale objects.

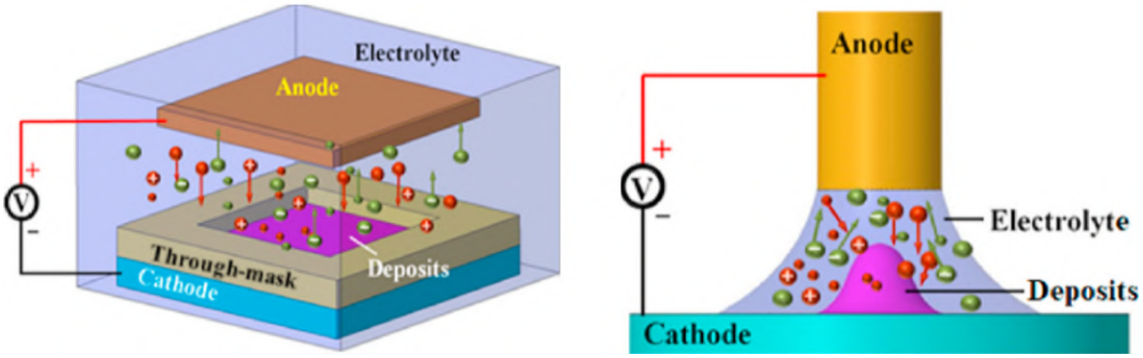

Figure 1.3: Schematic diagram of two kinds of ECAM, mask based (Left) and mask-less (Right). (Reproduced from Ref.[10] with permission from Elsevier)

Depending on the presence or absence of the mask ECAM can be divided into two categories. The mask based means usually have a prefabricated mask on the surface to be plated and followed by ECD[10]. In contrast, mask-less devices allow deposition on substrates with design freedom at confined area[11, 12, 13, 14]. It is worth to know that generally a desktop printer that could be modified as an ECAM printer is only cost tens thousands of SEK, which is way cheaper than the traditional AM devices.

1.1.4 Graphene related materials

Graphene, an innovative Two-Dimensional (2D) material, has draw attentions of various fields, for example, automation, electronics and energy storage industries[15]. It is a single layer of covalent bonded sp_2 hybridised carbon atoms in a honeycomb structure, as shown in Fig. 1.4.

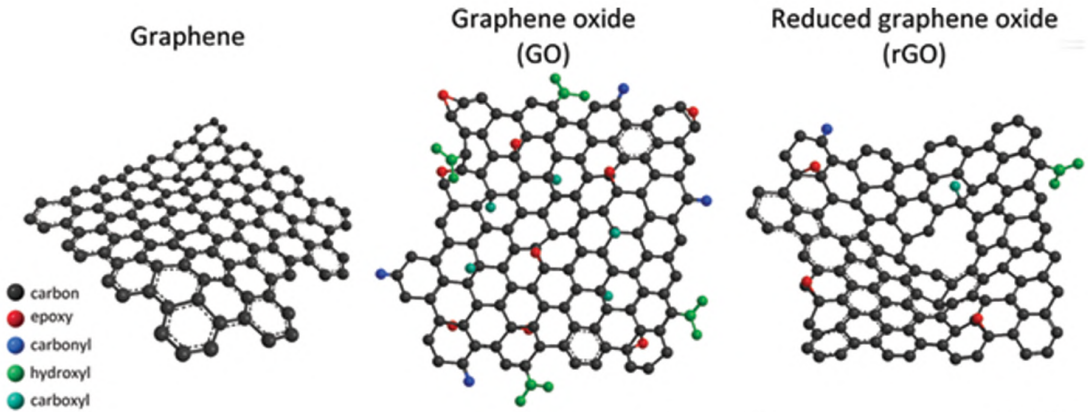

Figure 1.4: Schematic diagram of GO and rGO. (Reproduced from Ref.[16] with permission from MDPI)

Graphene Oxide (GO) and reduced Graphene Oxide (rGO) are both derivative materials of graphene. GO is mechanically exfoliated from graphite oxide and has

only one or few layers, like graphene does. rGO, as its name, is produced by reduction reaction from GO. In general, GO and rGO can improve the mechanical properties of composites by a homogeneous distribution, but due to the broken sp_2 bonding between carbon atoms by oxidation in GO it has distinctive electrical performance compared to rGO and graphene with a low electrical conductivity or a semi-conductive feature[17].On the other sides, graphene and rGO has more powerful van deu Waals forces between aromatic rings than GO. Hence, there's an issue that graphene always tends to agglomerate for reducing its surface energy, which means it's hard to be distributed in composite[18]. Additional, GO has a strong affinity for water while rGO repels water due to the loss of oxygen-containing functional groups during the reduction process. Consequently, GO is more easily dispersed and exhibits better colloidal properties compared to rGO[19].

1.1.5 Copper (Cu)

Copper (Cu) is a highly demanding material nowadays, especially in electronic industry[20, 21], and it is widely used in ECD[22] because of its superior performance at electrical and thermal conductivity and chemical stability. Cu is also a feasible material option for PBF methods but it has high reflection rate of laser which leads to higher energy consumption and potential harmful optical reflection leakage[20], although it could be solved with high penetrative electron beam in which leads to high energy consumption as well[23].

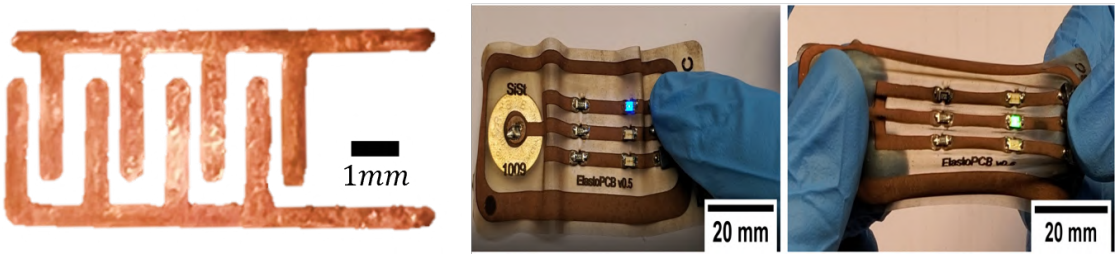

Figure 1.5: A pair of interdigitated electrodes made of pure Cu by ECAM (Left) and a stretchable circuit board made of Cu based material by ECD (Middle and right). (The image in the middle and on the right is reproduced from Ref.[24] with permission from MDPI)

More importantly, in terms of ECD, a green and low-cost technique to produce pure Cu, the combination of Cu and it attracts great attentions from both academia and industry in the field of electronic manufacturing in recent years[25], while other Cu production methods generate large amounts of waste, including sulphur dioxide, nitrogen oxides and particulate matter. And the Cu prepared by the ECD method does not reduce the purity, and it is still a versatile material widely applicable to various applications[22]. However, its weak mechanical performance make it unsuitable in certain working environment, especially under evaluate temperature[26]. Meanwhile, its pending corrosion resistance makes it unsuitable for certain operating environments, particularly at high temperatures and in humid environments. Furthermore, studies have shown that Cu composite is a necessary and efficient way

to strengthen Cu and its alloys, and the development of graphene-related material-reinforced Cu composites is a promising area of technology to be fully explored.

1.1.6 Cu/Graphene composites

As it mentioned above, Cu and its alloys have been widely utilised as structural materials in various engineering applications due to their exceptional properties such as high thermal and electrical conductivity, and excellent chemical stability. Nevertheless, the mechanical properties of copper and its alloys remain a significant limitation, particularly at high temperatures, which restricts their applications. Inserting a second phase into copper and its alloys to create Cu matrix composites has shown to be a viable technique for enhancing strength. Graphene has been used as a reinforcement phase to increase the mechanical capabilities of Cu while keeping outstanding thermal and electrical characteristics, resulting in improved structure-function integration.

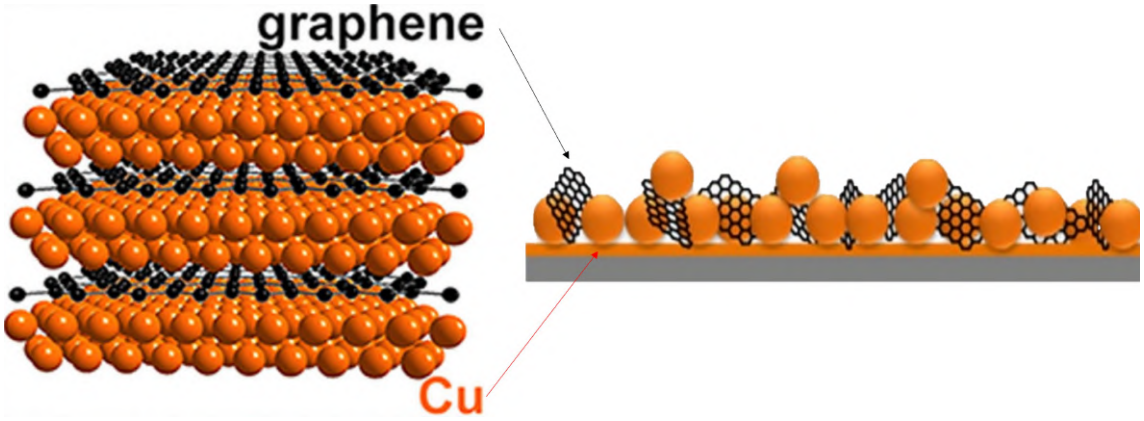

Figure 1.6: Schematic diagram of two structures of Cu/Graphene composites, layered (Left) and granular (Right), where the yellow spheres refer to Cu while the black mesh structure refers to graphene. (Reproduced from Ref.[27] and Ref.[28], respectively, with permission from Springer Nature)

Based on the findings of Chokkakula et al.[28], Li et al.[29] and Hwang et al.[27], Cu matrix can be significantly enhanced by granular graphene, in which graphene particles are embedded in a Cu base. Furthermore, Xiong et al.[30], Kim et al.[31] and Xiong et al.[32] demonstrated another common microstructures of Cu/graphene composites that Cu and graphene alternate in a layered structure.

1.2 Aim

This thesis work aims at the printing of graphene related metal composites by a desktop electrochemical 3D printer, which is a micron ECAM approach with a modified Fused Deposition Modelling (FDM) printer. The ultimate goal is to develop a low-cost, efficient and sustainable method that can be applied in various electronic manufacturing applications. Meanwhile, develop a Cu/GO composites which can

be produced by ECAM with homogeneous GO distribution and good anti-corrosion ability.

1.3 Approach

In this work, metallic composites with quasi 3D structures will be directly printed through the formation of a stabilised liquid meniscus between the dispensing nozzle and the conductive substrate. The key deposition parameters, device design, programming, power supply, substrates, and precursors, will be studied in this project to optimise the ECAM process as well as mechanical and electrical performance of composites. The morphology of the printed Cu/GO samples will be analysed using Scanning Electron Microscopy (SEM). The electrochemical properties of the samples will be characterised using Cyclic Voltammetry (CV) and anti-corrosion tests. Additionally, Raman Spectroscopy (Raman) and X-ray Photo-electron Spectroscopy (XPS) techniques will be explored to investigate the chemical elements. Eventually, micro-compression testing will be performed to testify the mechanical strengthen.

1.4 Limits

Several limitations need to be considered in this master thesis work. The first is the time limit. The project needed to be completed over several months, which limited the number of experiments and data collection that could be performed. In addition, technical limitations have to be considered, as there are some difficulties, i.e., the nozzle travel speed was limited by the printer's firmware, with the machines used for the research. Despite these challenges, the project will be carried out to the best of our ability to ensure the best possible outcome.

2
Theory

2.1 ECD principle

ECAM, in this thesis, is based on cathode ECD, a process that includes an electrolyte and two electrodes, an anode and a cathode. These two are required to be connected to the positive and negative terminals of an external power supply, respectively. Under the applied electric current, the metal ions in the electrolyte are moved by electric field forces, resulting in an electric current. Then, they are reduced to form metal atoms on the surface of the cathode, while the oxidation reactions happens on the anode[33]. The deposition occurs atom by atom, resulting in the growth of a metal layer on the cathode substrate. To be noticed, there are two kinds of the anode, sacrificial and permanent. As their name, the sacrificial one is made of same metal as the metal ion in electrolyte and dissoluble while the permanent one is made of inert metal which has no ions in common with the electrolyte[34].

2.1.1 Electrochemical reaction

The major steps happened on cathode during ECD is electrochemical reduction reaction, namely charge transfer[35] as shown in Eq. 2.1.

$$M \rightarrow M^{n+} + ne^{-} \tag{2.1}$$

where M is the metal and n is the number of electrons lost by M in the reduction reaction.
Together with liquid phase mass transfer, pre-conversion and electro-crystallisation, it constitutes a complete ECD process. Here, the detailed steps are given out.

1. Liquid phase mass transfer: Metal ions in the electrolyte move to the cathode surface.
2. Pre-conversion: Metal ions are adsorbed to the surface of the cathode and react electrochemically to form nuclei or clusters.
3. Charge transfer: Metal ions are reduced to metal atoms on the cathode surface.
4. Electro-crystallisation: Metal atoms deposited at the cathode start to grow and form a crystalline structure, resulting in the formation of a metallic layer of coating.

Meanwhile, oxidation could happen on the surface of sacrificial anode and it provides more metal ions and free electrons. Therefore, the reaction is described as Eq. 2.2.

$$M^{n+} + ne^{-} \rightarrow M \tag{2.2}$$

However, metal ions can be obtained not only from sacrificial anodes containing the same elements, but also from metal cations in the electrolyte.

2.2 ECAM principle

As previously described, ECAM is a technology that is urgently needed now and has a wide market potential. The current main processes can be divided into two categories based on the electrolyte supply method, relying on electrolyte bath and through confined meniscus (Electrolyte bridge), as shown in Fig. 2.1.

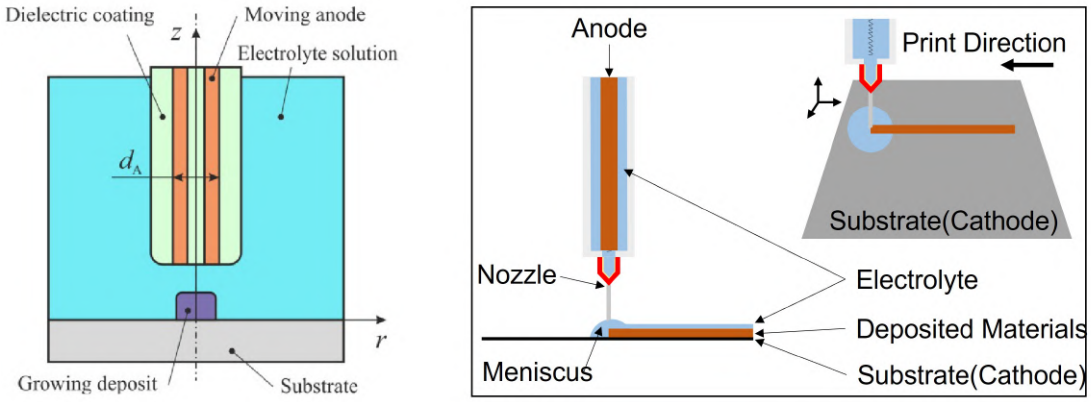

Figure 2.1: Schematic diagram of ECAM by electrolyte bath (Left) and through confined meniscus (Right). (The image on the left is reproduced from Ref.[13] with permission from Elsevier)

Both ECAM methods are based on a localised ECD process, so that the space between the anode and cathode can be considered as an electrolytic cell with a power source, which operates essentially the same as previously described in the ECD principles. On this basis, the anode can move freely as the print head of 3D printer in the printing room (The space above substrate) and deposit metal ions on the cathode in real time by means of a pre-designed model controlled by computer software.

3

Methods

3.1 Setup design

The setup consisted of a modified industry 3D printer (ZYYX Pro, ZYYX Labs) and a Direct Current (DC) power supply (2260B-250-4, Keithley). A syringe holder was produced by ZYYX labs AB using Nylon. The syringe (5100-X00V0, Henke Sass Wolf) was a 10 mL (12 mL) version with Luer lock for use with an insulated nozzle (925125-DHUV, Metcal) with an inner diameter of 0.25 mm. The anode and the fixed substrate (cathode) were connected to the power supply with two crocodile clamp and connecting wires, as shown in Fig. 3.1.

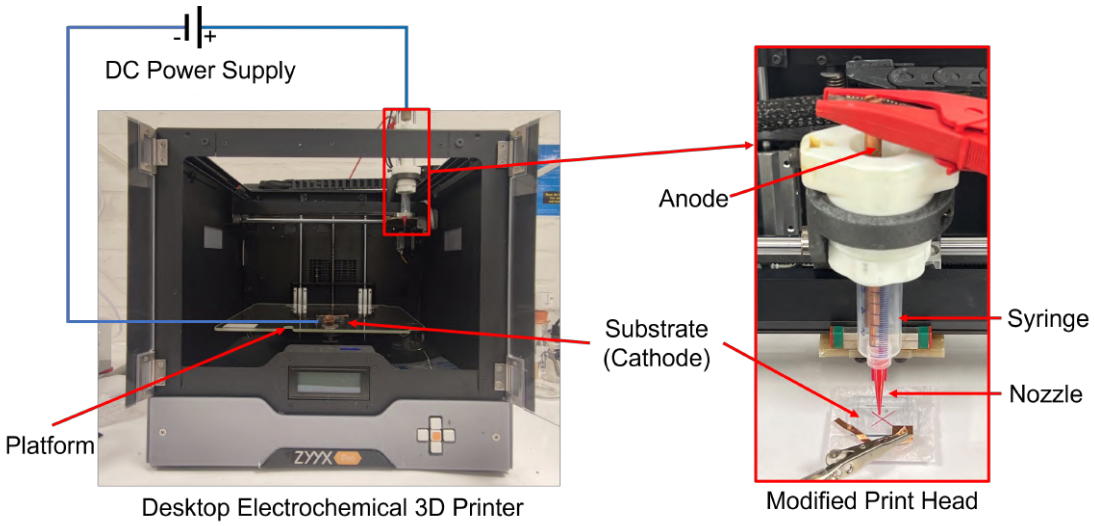

Figure 3.1: The modified desktop 3D printer and its print head.

3.1.1 Programming

A CAD model needed to be designed and built first and then transferred to a Standard Triangle Language (STL) file that can be recognised by the slicing software. The Geometric Code (G-code), a language that can be understood and executed by machines, could therefore be generated and fed into the 3D printer via the Simplify3D software. Based on this, the enclosed ECD started depositing material in a defined shape on the target substrate.
The fly-height, the height of the nozzle to the substrate surface, could be adjusted by computer software or manually moving the syringe in the Z direction and tightening

the bolt once a suitable height had been obtained.
The pattern design was to create a single straight lines of 8 mm.

Table 3.1: Parameters of programming.

Parameters	Values
Nozzle movement speed	1 mm/s
Total print time	30 minutes
Fly-height	100 - 200 μm

3.1.2 Power supply

Applied voltage was not the major research question in this work. Hence, 5 V was chose because it is widely used and proven and won't cause electrolytic water reaction during deposition[36]. Current was limited naturally by this deposition process, but in case of dangerous the upper limit of current was set to 0.01 mA at the power supply. A Digital Multi Meter (DMM) (175 True-RMS, Fluke) was used to measure current and resistance of the wire between anode/cathode and power supply.

3.2 Experiments

3.2.1 Materials

All materials and chemicals used in this paper are listed below in alphabetical order. In addition, all chemicals are of analytical grade and used in the experiments are not purified.

1. Benzotriazole (BTA), $C_6H_5N_3$, 99%, from Sigma-Aldrich.
2. Sodium Carboxymethyl Cellulose (CMC), average mW 250,000, degree of substitution 0.7, from Sigma-Aldrich.
3. Copper (Cu) foil, 99.99%.
4. Copper (Cu) rod electrode, 99.99%, diameter of 5 mm.
5. Copper(II) nitrate trihydrate, $Cu(NO_3)_2{\cdot}3H_2O$, 99-104%, from Sigma-Aldrich.
6. Copper sulphate, $CuSO_4 \cdot 5H_2O$, $\geq$ 99.8%, from Sigma-Aldrich.
7. Copper (Cu) wire, 99.99%, 0.5 mm^2.
8. Ethanol absolute, C_2H_5OH, $\geq$ 99.8%, from VWR.
9. Grphene Oxide water dispersion, 0.4 $wt.\%$, from Graphenea.
10. Highly Oriented Pyrolytic Graphite (HOPG), 12x12x2 mm, grade ZYH, from Momentive Performance Materials.
11. Hydrochloric acid fuming 37%, HCl, from Supelco.
12. Indium Tin Oxide (ITO) coated glass slide, square, 703192-10PAK, from Sigma-Aldrich.
13. Magnesium nitrate hexahydrate, $Mg(NO_3)_2 \cdot 6H_2O$, from Supelco.
14. Methyl Cellulose (MC), 400 cP, from Sigma-Aldrich.

15. Nitric acid 65%, HNO_3, from Supelco.
16. Poly(diallyldimethylammonium chloride) (PDDA) solution, $(C_8H_{16}ClN)_n$, 20 $wt.\%$ in water, from Sigma-Aldrich.
17. Polyvinyl Alcohol (PVA), 99-100% hydrolysed, approx. Molecular Weight (M.W.) 124,000, from Thermo Scientific.
18. Sodium chloride, $NaCl$, $\geq$ 99.8%, from VWR.
19. Sulfuric acid 95-97%, H_2SO_4, from Supelco.

3.2.2 Precursor formulation

In this paper, the precursor formulation experiments focus on the selection of salts with copper ions and the selection of thickeners.
Two Cu salts were considered, $CuSO_4$ and $Cu(NO_3)_2$. $CuSO_4$ is commonly used for ECD, while $Cu(NO_3)_2$ is an alternative with good compatibility with GO.
Three common and well-established thickeners are chosen, namely PVA, CMC and MC, which are non-toxic or low toxicity and are used in a large number of industrial applications, including household products, pharmaceuticals and food, etc. To be noticed that the CMC used here is its sodium salt, i.e. Sodium CMC. During the selection of thickener for precursor, three thickeners were mixed with two different copper salts to obtain six combinations as Table 3.2.

Table 3.2: Six combinations of Cu salts and thickeners.

Sample	Cu salt	Concentration(mol/L)	Thickener	Concentration(g/L)
PVA/CS	$CuSO_4$	0.5	PVA	100
CMC/CS	$CuSO_4$	0.5	CMC	25
MC/CS	$CuSO_4$	0.5	MC	25
PVA/CN	$Cu(NO_3)_2$	0.5	PVA	100
CMC/CN	$Cu(NO_3)_2$	0.5	CMC	25
MC/CN	$Cu(NO_3)_2$	0.5	MC	25

3.2.3 Preparation of precursors

In the advance study, the precursors formulation, also known as electrolyte formulation, was optimised based on the following principles. Firstly, $Cu(NO_3)_2$ was found to exhibit improved compatibility with GO due to its interaction with the graphene oxide material. Additionally, MC demonstrates excellent thickening ability in electrolyte solutions and shows good compatibility with $Cu(NO_3)_2$ due to the presence of methoxy groups[37, 38]. Then, the introduction of sulphate and hydrogen ions by H_2SO_4 can considerably enhance the ionic conductivity of the electrolyte[36, 39] to increasing current during ECAM for faster deposition rate. In addition, GO is functionalised by PDDA, which contains a large number of cations that provide a positive charge to the graphene oxide[40, 41]. The Mg ions are adsorbed around the edges of GO through electrostatic interaction[41]. As result, both of them can improve the deposition efficiency of GO.

Hence, in this thesis, the electrolyte formulations was based on 0.5 mol/L $Cu(NO_3)_2$ and GO that was ranging from 0.1 $wt.\%$ to 3.0 $wt.\%$ of Cu atom concentrations. It included the addition of four additives as well, which are summarised in Table 3.3.

Table 3.3: Selected additives of electrolyte preparation and their purpose.

Additive	Concentration	Purpose
MC	25 g/L	Increase viscosity
H_2SO_4	0.1 mol/L	Increase ionic conductivity
PDDA	3:8 to GO	Improve GO dispersion
$Mg(NO_3)_2$	1:1 to GO	Accelerate GO deposition

Table 3.4: The formulations of precursors.

Name	$Cu(NO_3)_2$ (mL)	H_2SO_4 (mol/L)	MC (g/L)	GO (mL)	PDDA (g/L)	$Mg(NO_3)_2$ (g/L)
Pure Cu	0.50	0.10	25.00	-	0.10	0.32
Cu/0.1GO	0.50	0.10	25.00	0.40	0.01	0.03
Cu/0.5GO	0.50	0.10	25.00	2.00	0.06	0.16
Cu/1.0GO	0.50	0.10	25.00	4.00	0.12	0.32
Cu/2.0GO	0.50	0.10	25.00	8.00	0.24	0.64
Cu/3.0GO	0.50	0.10	25.00	12.00	0.36	0.96
Cu/3.0GO-NPB	0.50	0.10	25.00	12.00	-	0.96
3.0GO@Cu	-	-	-	12.00	-	-

The specific electrolyte preparation process was as follows. Firstly, sulphuric acid was added drop-wise to 10 mL of deionised water (Water), then copper nitrate hexahydrate and magnesium nitrate trihydrate were added successively and stirred well for the solution 1. Then 6.5 mL of ethanol absolute was added drop-wise to the MC powder and stirred well with a glass rod as the solution 2. Different amounts of GO was added to 10 mL of water and sonicated with an amplitude of 20% for 30 minutes using a tip sonicator (VCX-505, SONICS & MATERIALS) to obtain the solution 3. The solution 4, similarly PDDA was added to 10 mL of water and sonicated for 30 minutes using a tip sonicator, after which it was mixed with GO and sonicated again for 30 minutes using a tip sonicator. Solutions 1, 2 and 4 were mixed to obtain a GO-free printing precursor. Solutions 1, 2, 3 and 4 were mixed and spiked with water to 50 mL to obtain a GO-containing printing precursor. All precursors were well stirred after mixing using a glass stirring bar and were left to stand until free of air bubbles.
In addition to the normally prepared precursors, one more was prepared as a control following the steps below. Certain amount of GO was first taken and fixed with water to 50 mL, then sonicated for 30 minutes with a tip sonicator and subsequently cooled to room temperature and then reserved.

3.2.4 Substrates selection

A total of three base materials in this work were presented below, called Cu foil, HOPG and ITO coated glass slide, respectively(Hereinafter referred to as ITO).

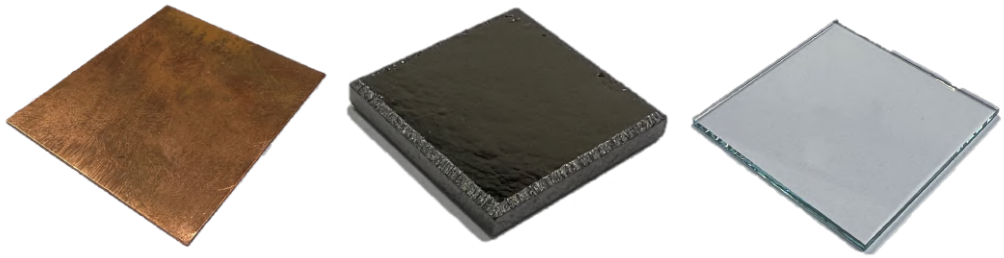

(a) Cu foil (b) HOPG (c) ITO

Figure 3.2: Three different substrates used in thesis work.

Cu foil was the first option, as the results in the lead project of this thesis shows pure Cu printing can be achieved on it. HOPG was considered as the second option because of its unique lamination property that has thin single layer with a thickness of few hundreds μm and could allow easier substrate removal without damaging the sample. Finally, ITO was chosen because it also has good conductive properties and was relatively flatter than HOPG.

3.2.5 Experimental design

Table 3.5: The detailed experimental design.

No.	Precursor	Substrate	Pattern	Propose
1	Pure Cu	Cu foil	8 mm line	Choice of substrate
2	Pure Cu	HOPG	8 mm line	
3	Pure Cu	ITO	8 mm line	
4	Cu/0.1GO	ITO	8 mm line	Study the influence of GO content
5	Cu/0.5GO	ITO	8 mm line	
6	Cu/1.0GO	ITO	8 mm line	
7	Cu/2.0GO	ITO	8 mm line	
8	Cu/3.0GO	ITO	8 mm line	
9	Cu/3.0GO-NPB	ITO	8 mm line	Study the influence of PDDA and BTA
10	3.0GO@Cu	Cu foil	-	Sample for control

In order to determine a stable fundamental more quickly, the first step was to select a durable, stable and reproducible one from the three substrates. This step was

performed with Pure Cu precursor without any GO content. Once the most suitable substrate had been selected, the optimised precursors were ready for printing. Then, the composites made of Cu and different concentrations of GO were printed. Additionally, three samples were made for investing the influence respectively from PDDA and BTA. And one sample was made as control group with only 3.0 $wt.\%$ GO on the surface for studying if rGO existed after ECAM. Finally, two demos were printed for exploring the design freedom degree and the potential application. The detailed experimental design is shown in Table 3.5. To be noticed, all samples were covered by BTA solution during printing and immersed into it for 10 minutes.

3.2.6 Manufacturing procedure

All laboratory supplies, especially conductive substrates, nozzles and syringes, and tools were cleaned before and after use, successively with ethanol and water. All experiments were conducted at room temperature. And the concentration of the BTA solution used during all works was 1 $mmol/L$.
The detailed steps of ECAM are listed as follows.

1. Anodes needed to be deep cleaned, sonicated with acetone, ethanol and water respectively. Then they were etched for one minute with etchant. The etching solution consists of 40% H_2SO_4 and 20% HNO_3 and 0.2% HCl, the remainder being water.
2. The conductive substrate was fixed with conductive Cu tape (1136, 3M) on the printer's platform and a simple connector was made to connect the negative terminal of power supply, see the right side of Fig. 3.1.
3. The nozzle and syringe were combined and then fastened in the syringe holder.
4. Without loading the electrolyte and install the anode, the unit was run in order to calibrate the fly-height. Fly-height can be estimated by inserting a sheet of A4 paper of known thickness between the substrate and the nozzle, measured by a digital vernier caliper.
5. Load 2 mL of the pre-configured electrolyte and insert the anode into the nozzle and connect it to the positive terminal of the power supply using a crocodile clamp.
6. Printing was started from the printer's control board or the computer software.
7. After three layers print, few drops (Depended on area of printing) of BTA solution were dropped to the surface of the deposition in order to prevent the electrolyte from drying out too quickly, clogging the nozzle and damaging the deposited parts.
8. When printing was complete, the printing process was terminated from the printer interactive interface or the computer software.
9. The sample was removed from the platform along with the substrate and washed by BTA solution. Then it was immersed in the BTA solution for ten minutes and dried in a vacuum oven (Glass Oven B-585, Buchi) at 40 $°C$.
10. The sample was placed in a vial and charged with only nitrogen to preserve it for characterisation or other testing purposes.

For preparing 3.0GO@Cu, a Cu foil was washed by successive acetone, ethanol and water firstly. Then a drop of the corresponding precursor was taken and then added

dropwise to the surface of the well cleaned Cu foil. After drying in a vacuum oven at 40 $°C$, it was finished.

3.3 Characterisation of deposits

As discussed in the experimental design section, Pure Cu was used as the control and the characterisation technique for the deposited samples was chosen based on three main claims. One was to analyse the changes in the surface morphology of the samples after the addition of GO and its effect on the Cu deposition. The second was to observe the distribution of GO and whether there was a possible rGO that was electrochemically reduced from GO. The third was to explore its application in the direction of energy storage. Ultimately, SEM, Raman, XPS, CV and Anti-corrosion were selected and performed.

3.3.1 Scanning electron microscopy (SEM)

SEM was used to observe and analyse the surface or fracture pattern of a sample by bombarding the surface of the sample with a fine focused electron beam, through the secondary and back-scattered electrons produced by the interaction of the electrons with the sample.
In this work, SEM imaging was performed by a JEOL JSM-7800F Prime. The top surface morphological features and thickness from cross-section of all samples were observed. During the test, the acceleration voltage was 2 kV or 5 kV under secondary electron mode, the LED was chose as detector and the working distance was 10.4 mm.

3.3.2 Raman spectroscopy (Raman)

Raman spectroscopy is a non-destructive analytical technique based on the interaction of light and chemical bonds within a material, providing detailed information on the chemical structure, phase and morphology, crystallinity and molecular interactions of a sample.
A WITec alpha300 R was used for Raman analysis to prove the existence and study the distribution of graphene-related materials. The excitation wavelength of laser source here was 532 nm and the power of laser was 1 mW. Both single point spectrum and mapping results were acquired under the 100× magnification of an Optical Microscopy (OM) and the numerical aperture was 0.9.

3.3.3 X-ray photo-electron spectroscopy (XPS)

XPS is a method of obtaining information about the chemical composition and valence of a material's surface by using X-rays to irradiate the surface of the sample, causing the atoms on the surface to produce photo-electrons, and measuring the energy and number of photo-electrons.
In all samples, the one, Cu/3.0GO, containing highest amounts of graphene related material were selected for XPS characterisation and a control, 3.0GO@Cu. Besides,

Cu/3.0GO-NPB was selected here for study the influence of BTA and PDDA to compositions.
A scanning XPS microprobe (PHI5000 VersaProbe III) was used here. The source was a monochromatic Aluminium (Al) $K\alpha$ X-ray with an energy of 1486.6 eV. The beam size diameter was set at 100 μm with a 25 W power and 15 kV voltage. Two scan modes were employed for the analysis. The first scan mode was a survey scan, which covered the energy range from 0 to 1300 eV with a step size of 1.00 eV. This scan was performed to evaluate the overall composition of the sample. The second scan mode was a narrow scan, conducted in selected regions of interest to analyse the chemical state. For C 1s element, the step size was 0.05 eV, while for others, it was set at 0.10 eV. The energy resolution achieved by a 100 μm beam, represented by the full width at half maximum was 0.654 eV. To ensure accurate analysis, the narrow scan measurements were aligned with the graphitic carbon peak (C 1s) at 284.6 eV. Lastly, the concentration detection limit of this XPS setup was determined to be 1.0 $at.\%$. This indicates that the XPS technique employed in this study can reliably detect elements present at concentrations above this limit.

3.3.4 Cyclic voltammetry (CV)

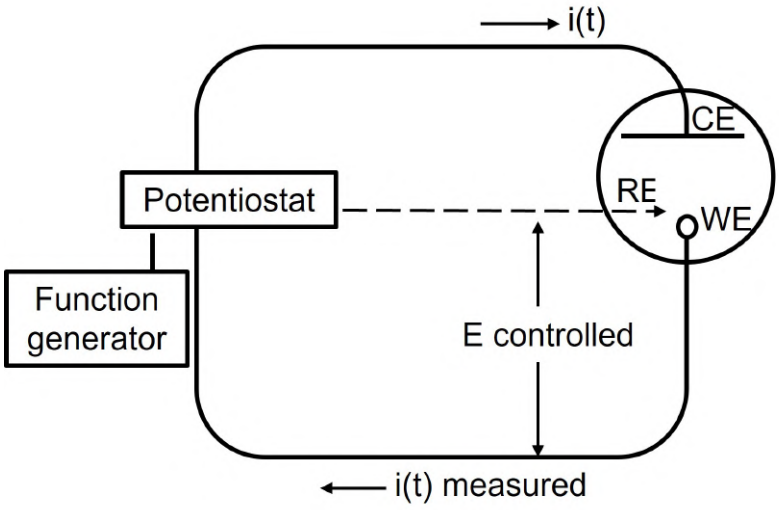

Figure 3.3: Schematic diagram of three electrodes method.

This test was performed with three cycles for each sample using a Bio-Logic SP-300 electrochemistry workstation with a scan rate of 100 mV/s between -0.5 V and 0 V and 0 V and 0.5 V.
CV is typically used to study the reactions and mechanisms at the electrode surface by applying a voltage to the electrode at a constant scanning rate and continuously observing the relationship between current and potential at the electrode surface.
The three electrodes method was used here as the test setup. A 5 mm^2 Working Electrode (WE) was exposed to an electroactive test solution, i.e. 1 mol/L, along with a Counter Electrode (CE) made of 99.99% Platinum (Pt) and a Reference Elec-

trode (RE), i.e. Ag/AgCl/KCl (sat'd), a silver chloride electrode for an electrolyte solution saturated with potassium chloride.

3.3.5 Anti-corrosion

Anti-corrosion tests were carried out to verify the corrosion resistance of Cu/GO composites under simulated seawater conditions. The setup was partly same as set in CV except the electroactive test solution. Here, the aerated 3.5% Sodium Chloride (NaCl) at pH 7 was chose instead[42]. Linear Polarisation Resistance (LPR), the specific test for anti-corrosion, the technique performs linear polarisation resistance testing according to ASTM-G59. The voltage change rate was 1 mV/s and the initial voltage was -1 V with respect to the reference electrode. The step percentage was 25% and the number of tests was 5. The measurement range was -1 V to 1 V with an automatically selected current range of 10 mA and a bandwidth of 7.

4

Results and Discussion

4.1 Precursors

Different dissolution methods were required for each of the three thickeners. For PVA, water was first added and then it had to be stirred for one hour at 150 $°C$ and 1000 rpm. For CMC, it is first dispersed in a small amount of ethanol and then stirred with water for one hour with a speed of 1000 rpm. For MC, it is first dispersed in a little ethanol and then added to water and stirred with a stir bar for one minute. Following the optimised addition concentrations mentioned in last chapter, the three solutions ended up with similar viscosity, as estimated by calculating the time of dropping from the nozzle.
$CuSO_4$ and $Cu(NO_3)_2$ were dissolved by water and without any specific treatment.

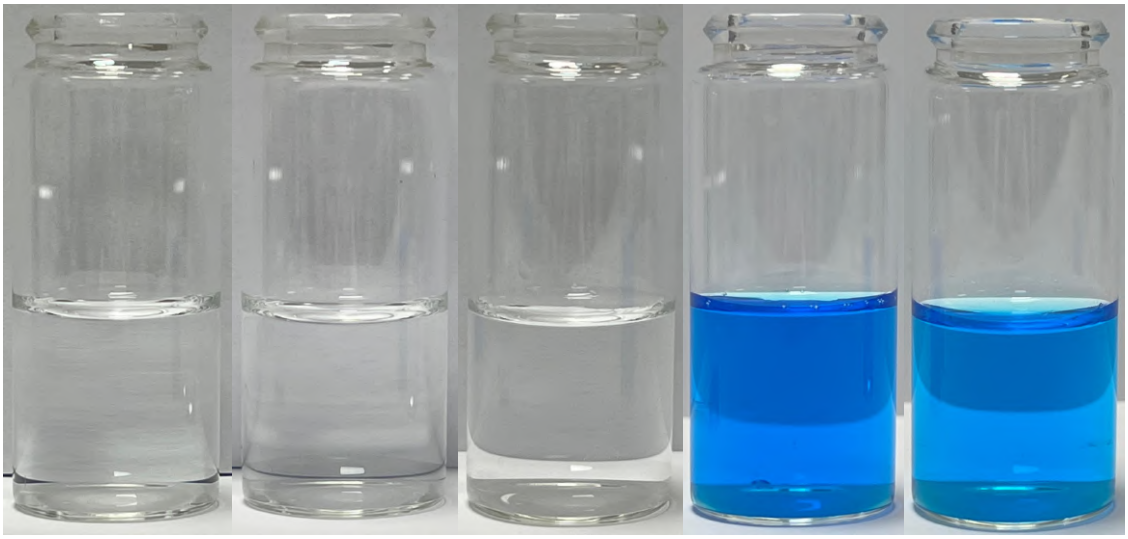

(a) PVA **(b)** CMC **(c)** MC **(d)** $CuSO_4$ **(e)** $Cu(NO_3)_2$

Figure 4.1: Solutions of two Cu salts and three thickeners before mixing.

Before mixing the different Cu salts and thickeners, the PVA, CMC and MC solutions all appear colourless and transparent when $CuSO_4$ and $Cu(NO_3)_2$ solutions have a similar light blue, the colour of the Cu(II)–water complex ion, as shown in Fig. 4.1.
After mixing, the six combinations from different Cu salts and thickeners were left to rest for 12 hours. Then there are only two combinations working, PVA/CN

and MC/CN, as shown in Fig. 4.2, and none of them precipitated, flocculated or agglomerated, while other four did.

(a) PVA/CS **(b)** CMC/CS **(c)** MC/CS **(d)** PVA/CN **(e)** CMC/CN **(f)** MC/CN

Figure 4.2: Solutions of six combinations of two Cu salts and three thickeners after mixing.

From the results, it appears that CMC is not at all compatible with salts containing Cu ions because of the possibility of metal chelation[43] and both PVA and MC formed precipitates or insoluble polymers to varying degrees with $CuSO_4$, probably due to exceeding the solubilisation capacity of PVA and MC for Cu ions[44, 45]. Both PVA and MC dissolved well with $Cu(NO_3)_2$ and formed gels of satisfactory viscosity. However, the dissolution of PVA requires long heating at 150 $°C$ and high speed stirring at 1000 rpm, making it more complex to use than MC, which requires only simple stirring to achieve the same results as PVA. Therefore, the combination of MC and copper nitrate was finally chosen for further experiments.

4.2 Substrates

Fig. 4.3 shows three iterative experiments of 8 mm line segments deposited on Cu foil, HOPG and ITO respectively. The samples (lines) on ITO have better macroscopic morphological characteristics with neat and smooth edges, while the lines are accompanied by randomly growing edges after growth on Cu foil and HOPG. In addition, the lines deposited on Cu foil are not easily removed and the bond between sample and substrate is too tight, while the lines on ITO can be easily removed and do not show uncontrolled morphology. Lastly, there are several distinct yellow wavy lines near the line deposited on HOPG, which are present on the edges of the mono-layer HOPG. And to be noticed that the HOPG has peel-able layer structure with weak tensile and bending strength as graphite.

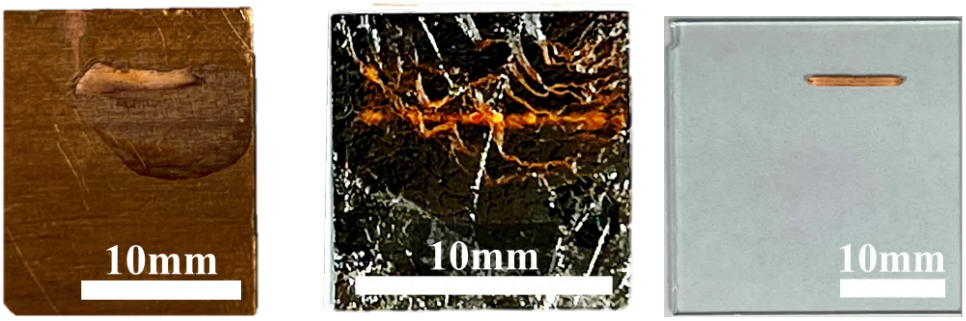

(a) On Cu foil **(b)** On HOPG **(c)** On ITO

Figure 4.3: Samples made of precursor, i.e. Pure Cu, on different substrates.

Experiments have shown that the surface of ITO only changes after 50 repeated uses, as shown in Fig. 4.4, specifically in terms of surface colour changes and localised contamination that is difficult to remove. All experiments were performed around the centre of ITO surface. Hence, the centre of the new ITO has the same colour as the outer part, while the centre gradually darkens compared to the outer part as it is used more times.

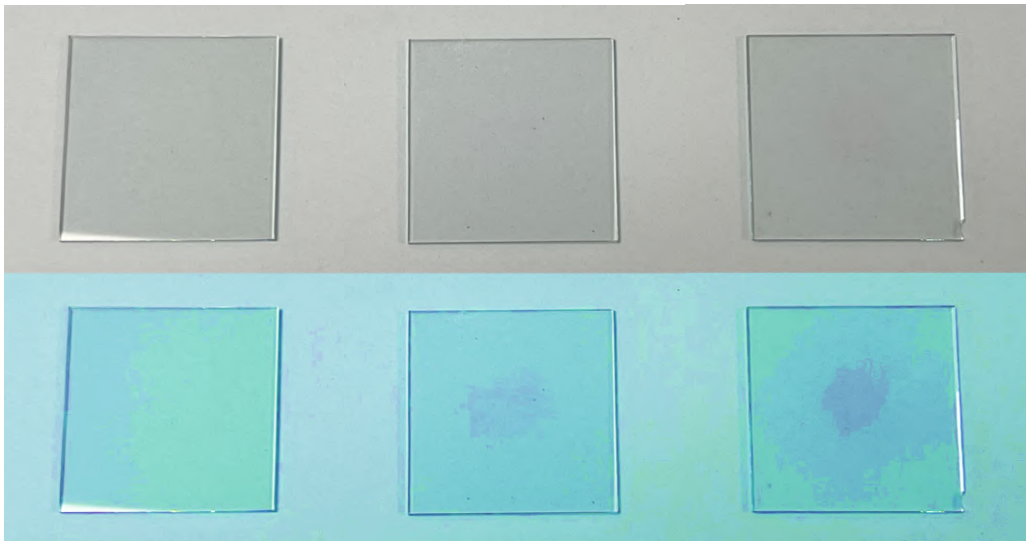

(a) Brand new **(b)** After 10 uses **(c)** After over 50 uses

Figure 4.4: Comparison of ITO surface of brand new state, after 10 times and after over 50 times printings. Photos at second row was modified by adoption of colour saturation from the original photos at first row.

In general, in terms of macroscopic morphology, the Cu foil and HOPG surfaces can be printed, but due to their different conductive properties and the differentiation of surface roughness[46, 47], the shape of the deposit presents irregularities and is difficult to separate after printing. For Cu foil in particular, the surface flatness is influenced by the processing accuracy, resulting in a very tight bond between the surface and the deposit after printing, which leads to a potential risk of damage to

the sample and limits the range of possible references, which means that the sample has to be used with Cu foil. For HOPG, the surface flatness is very good, but its reusability is poor and the graphite in the laminate structure is easily damaged, thus exposing the edges of multiple layers of graphite on the surface. It is known that graphite has a stronger electrical conductivity along the direction parallel to the carbon hexagonal ring than perpendicular to it, so during deposition Cu ions are deposited more efficiently at the edges of the graphite layers than at other locations, which in turn leads to a distribution along the edges that is uncontrollable and undesirable.
ITO has good reusability, easy separation from the deposit and a high surface flatness compared to Cu foil and HOPG, and is naturally the most suitable material for the time being for this work.

4.3 Deposits of pure Cu and Cu/Graphene Oxide (GO) composites

Results from seven samples, Pure Cu, Cu/0.1GO, Cu/0.5GO, Cu/1.0GO, Cu/2.0GO, Cu/3.0GO and 3.0GO@Cu were generally characterised and their precursors and manufacturing process followed the means introduced in Chapter Methods.

4.3.1 Surface morphology

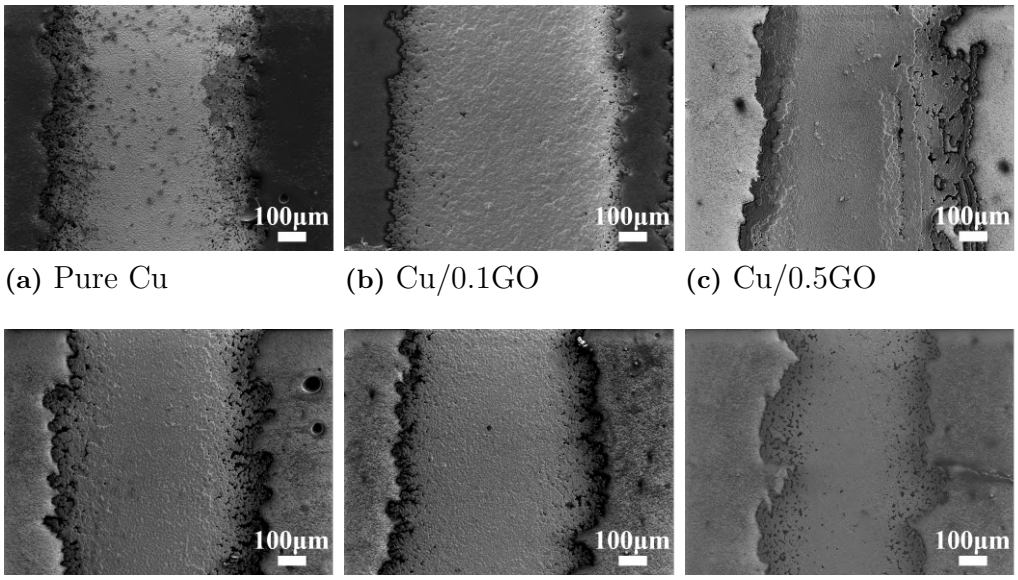

(a) Pure Cu **(b)** Cu/0.1GO **(c)** Cu/0.5GO

(d) Cu/1.0GO **(e)** Cu/2.0GO **(f)** Cu/3.0GO

Figure 4.5: 100× resolution SEM images of samples from Pure Cu, Cu/0.1GO, Cu/0.5GO, Cu/1.0GO, Cu/2.0GO and Cu/3.0GO.

From a surface perspective with 100× SEM images in Fig. 4.5, with the increasing of GO content, the smoothness of the sample surface improves and accompanied by

an increase in defects such as cracks and voids. In samples with GO content ≥ 0.5 $wt.\%$, irregular growth is evident on both sides of the line. Although there are also rough edges in the lines with GO content < 0.5 $wt.\%$, their degrees of roughness are less pronounced. Besides, there are some black spots protruding from the surface on all samples, in which could be ascribed to its faster oxidation rate than flat areas in storage.

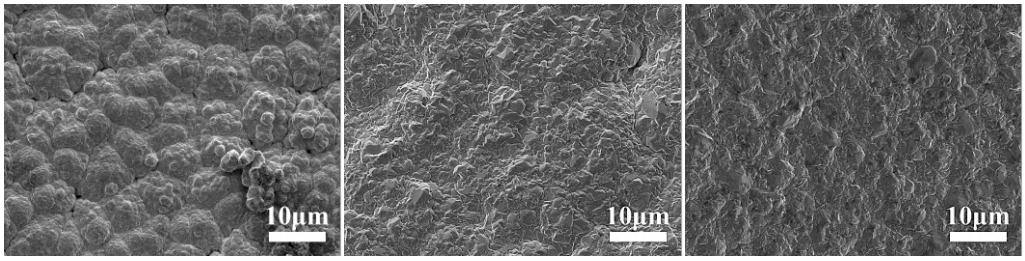

(a) Pure Cu **(b)** Cu/0.1GO **(c)** Cu/0.5GO

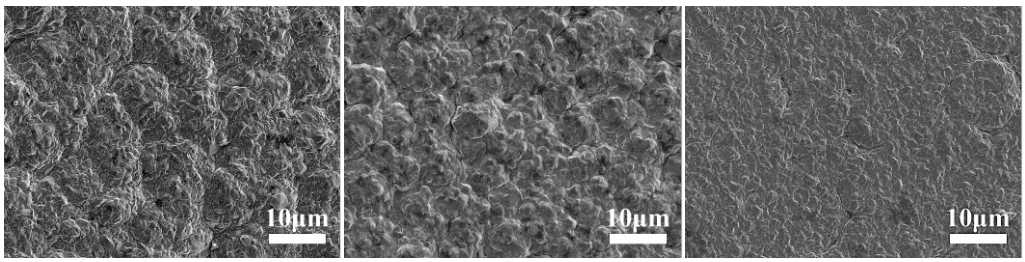

(d) Cu/1.0GO **(e)** Cu/2.0GO **(f)** Cu/3.0GO

Figure 4.6: 2000× resolution SEM images of samples from Pure Cu, Cu/0.1GO, Cu/0.5GO, Cu/1.0GO, Cu/2.0GO and Cu/3.0GO.

As shown in Fig. 4.6, the surface of Pure Cu is composed of individual hemispheres, whereas the surface of the GO addition consists of hilly-like bumps. In particular, the surface of Cu/3.0GO is generally smooth but with more visible cracks. The surface of the deposits is smoother with the addition of GO, but no specific trend is observed by different GO contents.

Whether it is the hemispherical structure of Pure Cu or the hilly structure of the Cu/GO samples, they are both composed of crystals of Cu, as presented in Fig. 4.7. The difference is that the grain size of Cu changes with the addition of GO to the precursors. With Pure Cu it has a Cu grain size of approximately 0.5 μm, while the rest of the GO containing precursor produces a grain size of approximately 1 μm.

In summary, in a series of SEM photographs it shows that the surface profile of the sample becomes flatter after the addition of GO, but at the same time there is a characteristic increase in grain size. There is no obvious GO or rGO on the surface, and there is also a problem with blurring of the surface morphology when the magnification resolution exceeds 20,000× during SEM observations. It is assumed that the BTA post-treatment has resulted in the formation of a poorly conductive BTA film on the surface of the deposits[48], which affects the electron signal during SEM observations.

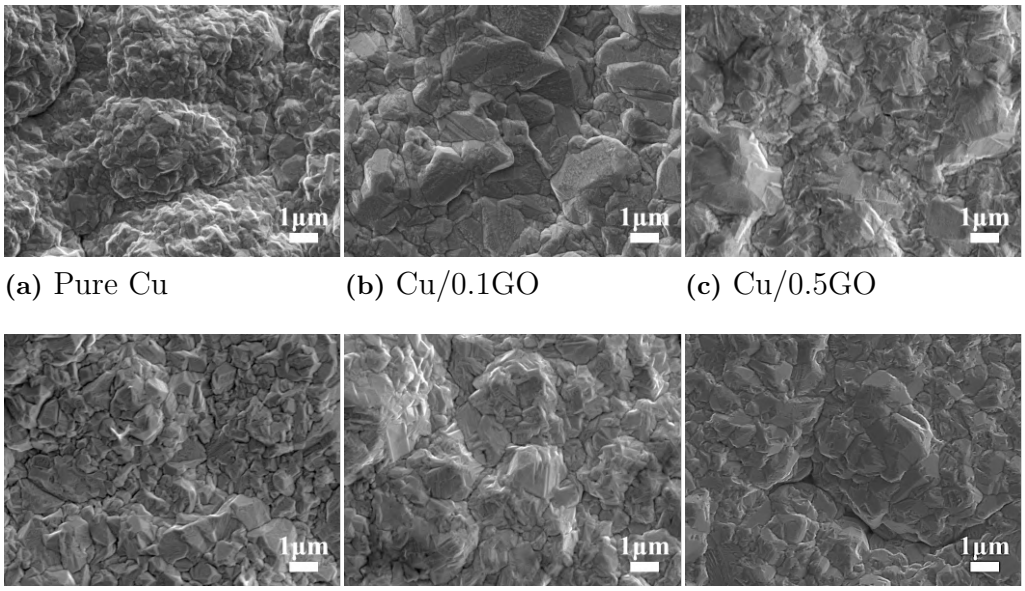

(a) Pure Cu **(b)** Cu/0.1GO **(c)** Cu/0.5GO

(d) Cu/1.0GO **(e)** Cu/2.0GO **(f)** Cu/3.0GO

Figure 4.7: 10,000× resolution SEM images of samples from Pure Cu, Cu/0.1GO, Cu/0.5GO, Cu/1.0GO, Cu/2.0GO and Cu/3.0GO.

4.3.2 Composition distribution and content

In this part, Raman and XPS were used successively as characterisation. First, Raman gave the distribution of graphene related materials and helped to classify its kind. Then, to further investigate the proprieties of GO and whether GO is reduced to rGO, XPS analysis was employed.

4.3.2.1 Raman spectrum and mapping

Looking into at a series of Raman mapping results, in Fig. 4.8, it is easy to see that the total graphene related materials content gradually increases as the GO content in the precursor increases. In addition, the graphene related materials distribution becomes increasingly homogeneous.

All samples were then analysed for the points containing graphene related materials, with the following results in Fig. 4.9. It demonstrates that GO and/or rGO exists in all samples prepared with GO content. The intensities of D band ($\approx 1354\ cm^{-1}$) and G band ($\approx 1603\ cm^{-1}$) are relatively large and comparable. The sp^2 C, Carbon (C) with sp^2 hybridised atomic orbital, is a common feature of GO and rGO in Raman spectrum and can be represented by the D and G bands[49], which means that GO and/or rGO is found in all the samples but in the Pure Cu. Here, the intensity ratio of D band and G band, I_D/I_G, are varying from 0.98 to 1.07, as shown in Fig. 4.9.

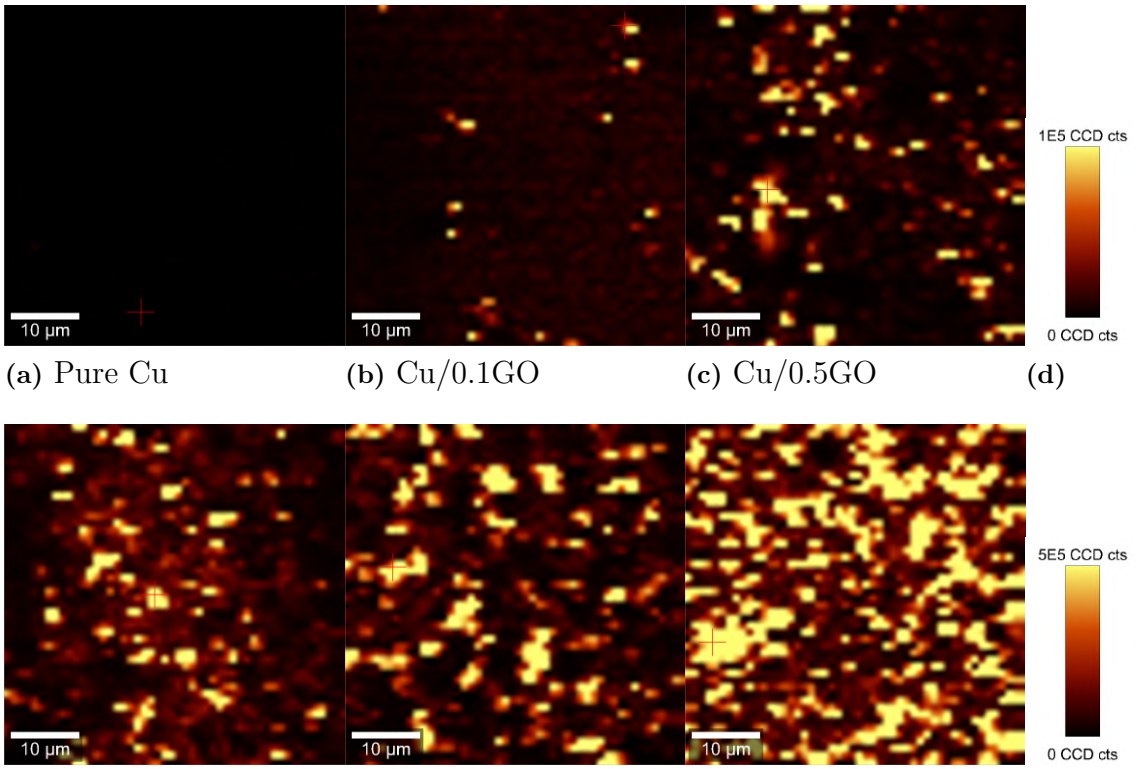

(a) Pure Cu **(b)** Cu/0.1GO **(c)** Cu/0.5GO **(d)**

(e) Cu/1.0GO **(f)** Cu/2.0GO **(g)** Cu/3.0GO **(h)**

Figure 4.8: Raman mapping of samples with different GO contents. (a), (b) and (c) refer to the scale in (d), and (e), (f) and (g) refer to the scale in (h).

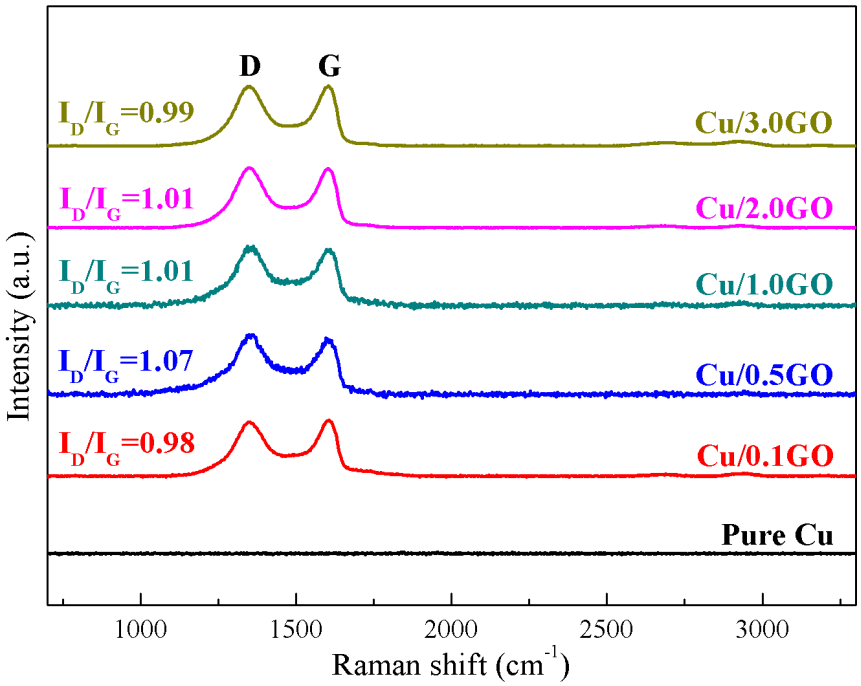

Figure 4.9: Raman spectrum of samples with different GO contents.

The Raman and dot spectra show that the GO/rGO content of the sample surface distribution increases with increasing GO content in the precursor and no excessive defects are found in them. Specifically, in well-organised graphene, D band refers to the lattice defects and G band refers to the phonon vibration of sp^2 C[50]. Besides, GO formed by oxidation reaction leads to defects by inserting of oxygen atoms, forming of Carbon (C)-Oxygen (O) compounds and breaking of graphene structure. Hence, the I_D/I_G ratio indicates the defect density in GO, such as loss of carbon atoms, introduction of impurity atoms or disorder of lattice structure[51]. Combined with the XPS spectral results, this further corroborates the presence of GO.

4.3.2.2 XPS pattern

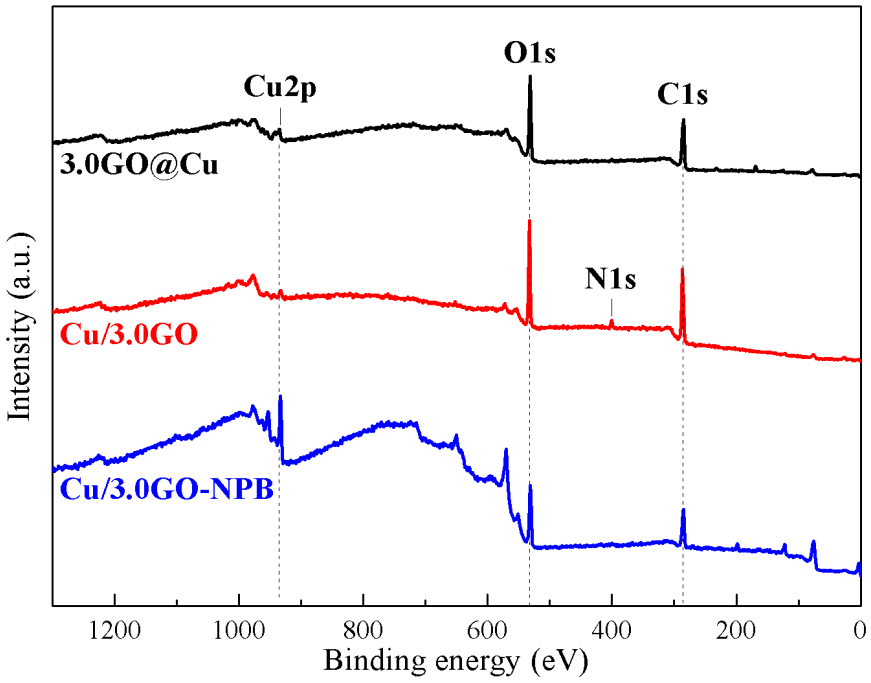

Figure 4.10: XPS survey spectra of Cu/3.0GO, 3.0GO@Cu and Cu/3.0GO-NPB.

Samples were further analysed by XPS to assess the chemical state of the various elements and the presence of functional groups. The survey spectra of all samples showed in Fig. 4.10. The predominant presence of C and O and Cu is found in all three samples here, while Cu/3.0GO has additional trace of Nitrogen (N).

High-resolution deconvoluted XPS spectra of the C 1s, O 1s and Cu 2p regions of Cu/3.0GO, 3.0GO@Cu and Cu/3.0GO-NPB are shown in Fig. 4.11, 4.12 and 4.13, respectively. C 1s spectra of three samples were deconvoluted into four component peaks corresponding to characteristic C bonds, C-C (sp^2 C bond,284.6 eV), C-O (286.5 eV), O-C-O (288.0 eV) and C=O (288.5 eV). O 1s spectra of them were deconvoluted into four component peaks as well, which corresponding to characteristic O bonds, M-O (530.5 eV), C=O (531.0 eV), C-O (532.6 eV) and R-OH (533.5 eV).

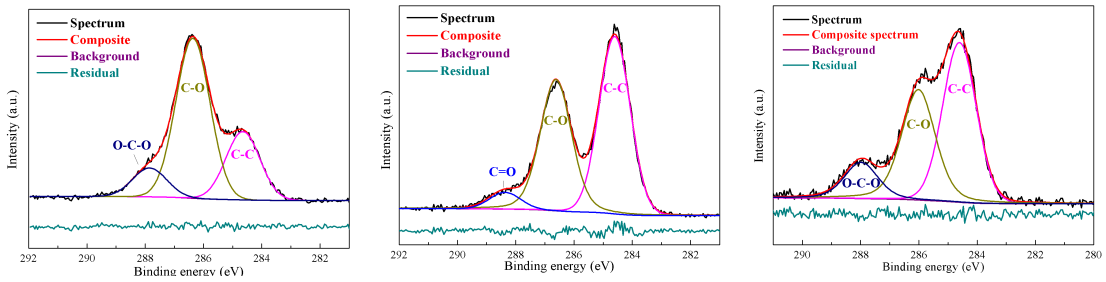

(a) Cu/3.0GO **(b)** 3.0GO@Cu **(c)** Cu/3.0GO-NPB

Figure 4.11: The deconvoluted XPS spectra of C 1s region from Cu/3.0GO, 3.0GO@Cu and Cu/3.0GO-NPB.

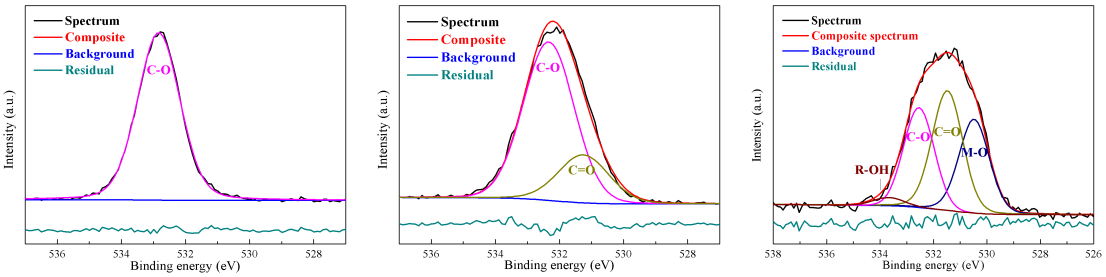

(a) Cu/3.0GO **(b)** 3.0GO@Cu **(c)** Cu/3.0GO-NPB

Figure 4.12: The deconvoluted XPS spectra of O 1s region from Cu/3.0GO, 3.0GO@Cu and Cu/3.0GO-NPB.

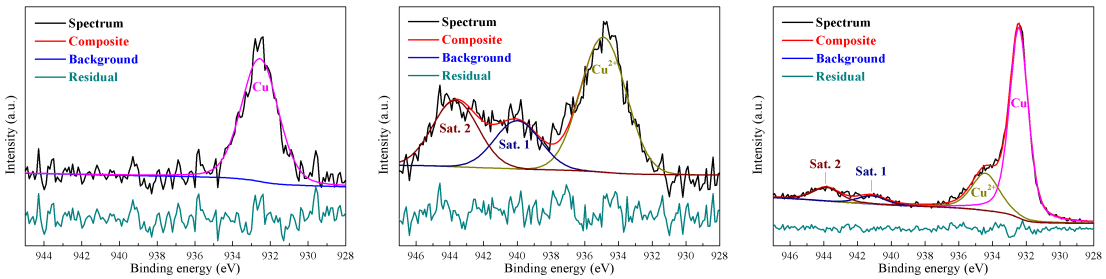

(a) Cu/3.0GO **(b)** 3.0GO@Cu **(c)** Cu/3.0GO-NPB

Figure 4.13: The deconvoluted XPS spectra of Cu 2p region from Cu/3.0GO, 3.0GO@Cu and Cu/3.0GO-NPB.

The detailed binding energies, the corresponding chemical bonds and the percentage of bonds from C 1s, O 1s and Cu 2p XPS spectra are listed in Table 4.2.

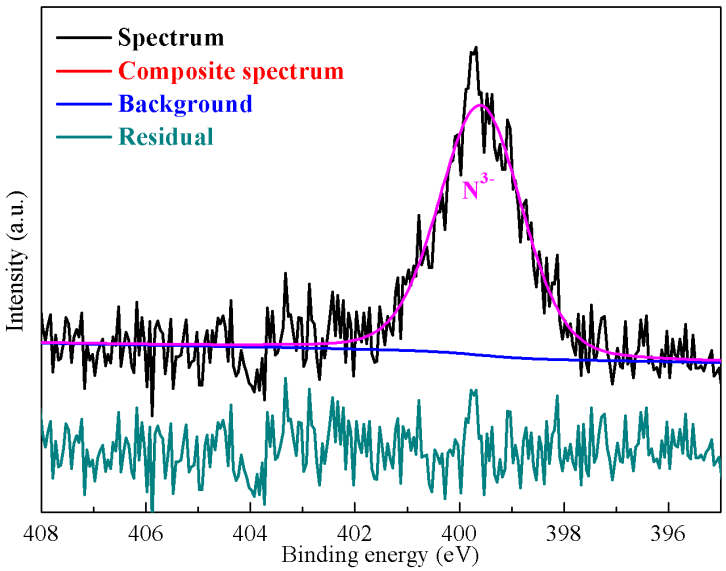

Figure 4.14: The deconvoluted XPS spectra of N 1s region from Cu/3.0GO.

To be noticed, a N 1s peak is found in Cu/3.0GO and it's corresponding to the exist of BTA[52], a common corrosion inhibitor for Cu. Hence, the BTA film that covered the composite formed on the surface of Cu/3.0GO.

Table 4.1: XPS chemical state analysis of C 1s region of Cu/3.0GO, 3.0GO@Cu and Cu/3.0GO-NPB.

	C 1s				O 1s				Cu 2p		N 1s
Binding energy(eV)	284.6	286.5	288.0	288.5	530.5	531.0	532.6	533.5	932.5	934.5	399.6
Bond type	C-C (sp^2)	C-O	O-C-O	C=O	M-O	C=O	C-O	R-OH	Cu	Cu^{2+}	N^{3+}
Cu/3.0GO	16.5%	39.0%	7.5%	-	-	-	32.0%	-	1.5%	-	3.5%
3.0GO@Cu	32.0%	25.5%	-	3.0%	-	8.5%	26.0%	-	-	3.0%	-
Cu/3.0GO-NPB	27.5%	21.0%	-	7.0%	10.5%	13.5%	10.5%	1.0%	5.0%	2.0%	-

Table 4.2: Surface compositions of Cu/3.0GO, 3.0GO@Cu and Cu/3.0GO-NPB from XPS.

Sample	C($at.\%$)	O($at.\%$)	Cu($at.\%$)	N($at.\%$)
Cu/3.0GO	60.5	34.5	3.0	3.5
3.0GO@Cu	63.0	32.0	1.5	-
Cu/3.0GO-NPB	55.5	35.0	7.0	-

The quantified atomic concentrations of C, O, Cu and N were calculated using XPS analysis, as shown in Table 4.2. In general, C content is rather at the same level in Cu/3.0GO and 3.0GO@Cu, i.e. 60.5 $at.\%$ and 63.0 $at.\%$ respectively, as well as O content, 34.5% and 32.0% in Cu/3.0GO and 3.0GO@Cu, but the level of C in Cu/3.0GO-NPB is less than other two samples while it has higher content of O and Cu. As we know, BTA is helping Cu to avoid from corrosion in air, oxidation

of Cu, and forms a thin film on samples surface. It could result to that photon-electron of XPS cannot fully penetrate the BTA film. Hence, more Cu is detected in Cu/3.0GO-NPB and more oxidation of Cu happened there. And for Cu/3.0GO, with the coverage of BTA, Cu is hided under the BTA film and Cu content is only 3.0 *at.*%.
The results shown in XPS indicate that the C-C (sp^2) bond content of the sample decreases and the C-O content increases after deposition, but the overall C and O content does not change significantly. And the larger proportion of C and O exists in both two samples with a small amount of Cu. (Fig. 4.10). It is speculated that the difference of sp^2 C bond may have originated from BTA or even PDDA additions.

4.3.3 Electrochemical properties

The electrochemical performance test section is divided into two parts, one is the CV test, which is to determine the electrochemical activity of the deposit and to test its ability to react with substances in solution during the electrochemical process as well as the redox reaction of the deposit and its mechanism. The second is the corrosion resistance test, in order to see how Pure Cu behaves against corrosion and whether or not the Cu/GO composite has an enhancement on the corrosion resistance.

4.3.3.1 CV diagrams

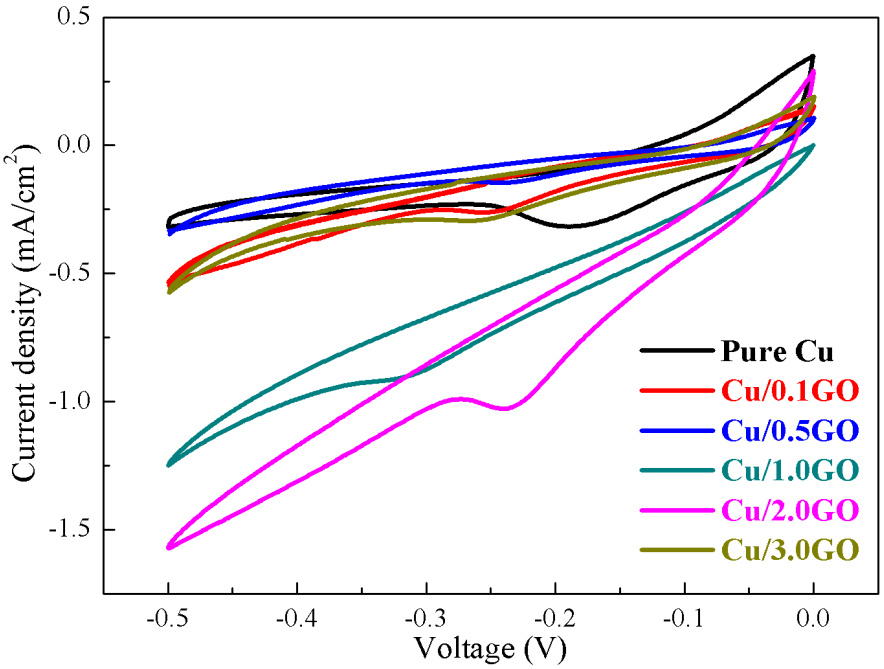

Figure 4.15: Cyclic voltammetry test results of samples with different GO contents from -0.5 to 0 *V*.

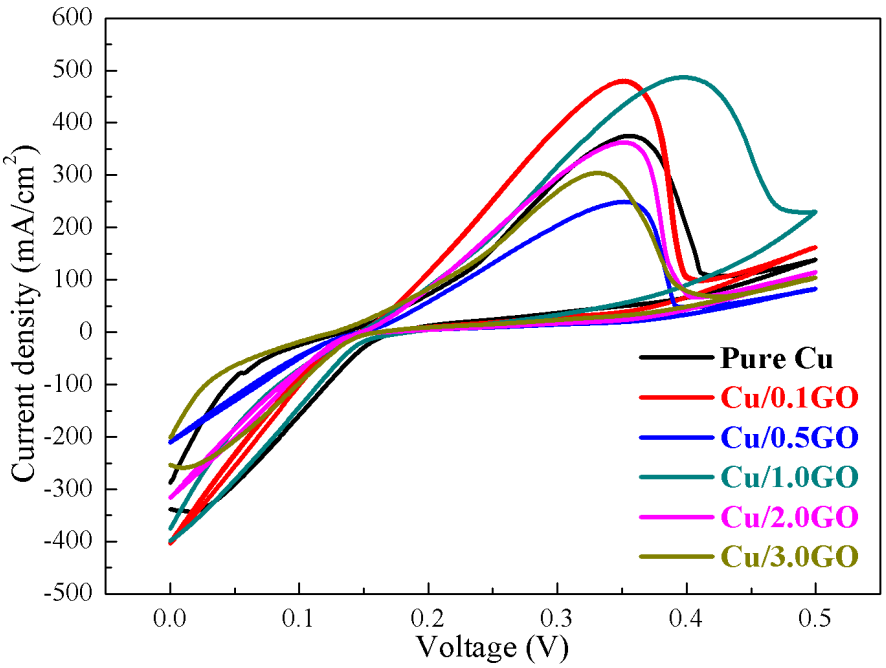

Figure 4.16: Cyclic voltammetry test results of samples with different GO contents from 0 to 0.5 V.

Fig. 4.15 shows the CV curves for samples with different GO contents. Typical reduction peaks were observed for all samples during the anodic scan for Cu^+/Cu[53, 54] at a scan rate of 100 mV/s over a voltage range of -0.5 to 0 V. The cathodic peaks (reduction peaks) are observed at all curves within -0.3 to -0.2 V. The shape of the cathodic peaks are similar but the current density and the potential of them are clearly different. In terms of adding GO in precursors, there is a significant change of potential of cathodic peak, which the reduction peaks from all samples with GO shifts to the left compared to Pure Cu, changed from -0.20 V to around -0.27 V (range from -0.25 to -0.30 V). And there is no reduction peak, indicating that the samples have an irreversible reaction as a working electrode and that GO helps to delay the reduction of Cu.
Then, a CV scan with a rate of 100 mV/s over a voltage range of 0 to 0.5 V was used for Cu^+/Cu and the result is shown in Fig. 4.16. The anodic peaks (oxidation peaks) are present at the potential around 0.35 V for all samples except for the Cu/1.0GO sample, around 0.4 V. The current densities of them ranges from 200 to 470 mA/cm^2. To be noticed, there is no reduction peaks showing up and this CV result is determined as an irreversible reaction. The GO doesn't establish significant help to facilitate or deter the oxidation reaction.
The behaviour of oxidation and reduction of Cu can be explained on the basis of the accepted mechanism for the dissolution of Cu in chloride (Cl^-) media, i.e. 1 mol/L KCl, as described in Eq. 4.1 and 4.2.

$$Cu + Cl^- \leftrightarrow CuCl^- + e^- \tag{4.1}$$

$$CuCl^- + Cl^- \leftrightarrow CuCl^{2-} \tag{4.2}$$

When Cu is exposed to a solution containing Cl^- ions, it dissolves as Cu^+ ions, i.e. $CuCl^{2-}$, a thermodynamic stable complex[53, 54]. Besides, there is not sign of reduction reaction of GO[55] in both CV diagrams, which means GO is stable in this composites under applied electric field.

4.3.3.2 Anti-corrosion ability

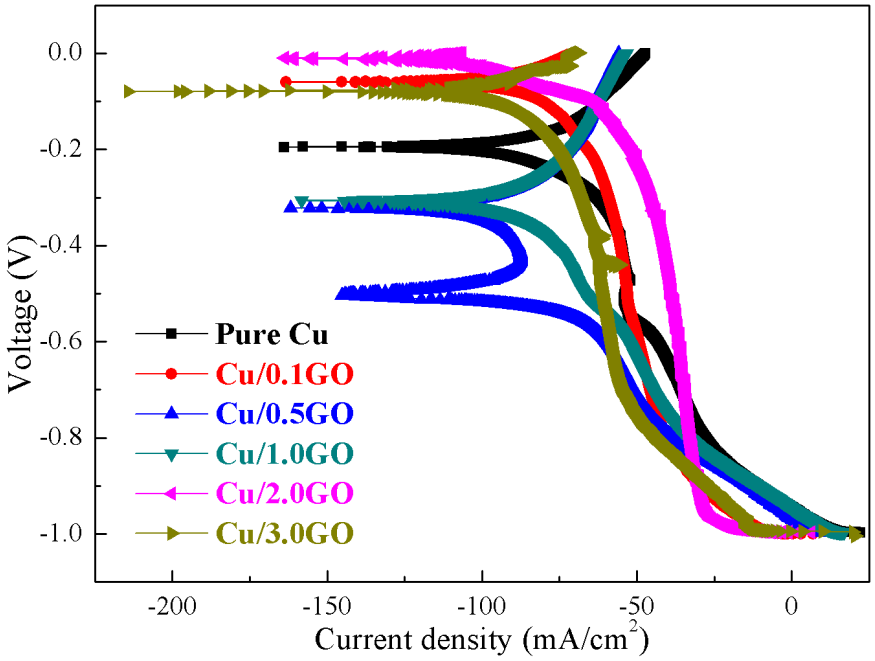

Figure 4.17: LPR curves obtained from samples with different GO contents.

As shown in Fig. 4.17, electrochemical corrosion behaviour of all samples were determined by LPR test. Additionally, tefal polarisation fitting was performed and the corrosion parameters, including corrosion current density (i_{corr}) and Tafel slopes (β_c for cathodic reaction and β_a for anodic reaction), were derived from it are presented in Table 4.3.

In addition, in Fig. 4.17, using the self-corrosive potential for Pure Cu the LPR curve as a reference (-0.195 V), it can be observed that Cu/0.1GO, Cu/2.0GO and Cu/3.0GO have higher self-corrosive potential, with values of -0.060 V, -0.010 V and -0.079 V respectively, while Cu/0.5GO and Cu/1.0GO are lower, showing potential of -0.322 V and -0.307 V respectively. Regarding the current density, only Cu/3.0GO is close to -210 mA/cm^2, the rest remain around -160 mA/cm^2. In addition, the curve for Cu/0.5GO has another peak in addition to the self-corrosion potential.

For further investigating the value of GO doping and digitising it, the corrosion inhibition efficiency (IE) is calculated according to Eq. 4.3,

$$IE = \frac{i^0_{corr} - i_{corr}}{i^0_{corr}} \times 100\% \tag{4.3}$$

, where i^0_{corr} and i_{corr} represent the corrosion current density of electrodes made of Pure Cu and Cu/GO composites respectively. Eventually, the IE values from all samples are listed in Table 4.3.
According to Table 4.3, E_{corr} values are irregular for samples with different GO content, while i_{corr} values of samples with GO decrease, varies from 1.928 to 4.111 mA/cm^2, compared to Pure Cu, 5.602 mA/cm^2. Additionally, the IE values from Cu/GO samples are all positive.

Table 4.3: Electrochemical corrosion parameters of samples with different GO contents derived Tafel tests.

Samples	$\beta_c(mV)$	$\beta_a(mV)$	$E_{corr}(mV)$	$i_{corr}(mA/cm^2)$	IE(%)
Pure Cu	215.1	334.5	-180.2	186.7	-
Cu/0.1GO	90.2	319.9	-31.7	103.6	44.5
Cu/0.5GO	352.0	144.0	-384.9	64.3	65.6
Cu/1.0GO	315.9	361.2	-316.1	103.6	44.5
Cu/2.0GO	18.7	256.9	15.1	137.0	26.6
Cu/3.0GO	116.0	380.6	-65.8	79.7	57.3

Based on the results of the polarisation curves and the Tafel fit, it is easy to see that GO enhances the corrosion resistance, but there is no direct correlation between GO content and the enhancement effect. Possible reasons for this are the corrosion resistance gain of the BTA film on the sample surface and the difference in surface morphology of the samples. In a number of studies, the surface morphology has been shown to have a crucial influence on the corrosion resistance of the product, as defects such as roughness, holes and cracks can directly accelerate the oxidation process of Cu[56].

5

Conclusion

In summary, this thesis reports on a low-cost ECAM method for the fabrication of Cu/GO composites. The preparation of Cu/GO composites was accomplished by an ECAM technique based on the ECD principle, consisting of a gel precursor consisting of copper nitrate and MC as a substrate with the addition of sulphuric acid, PDDA and magnesium nitrate, and the introduction of different levels of GO. The highlight of this work is the introduction of GO to enhance the electrochemical properties of Pure Cu, which introduces new ideas to improve the corrosion resistance of electrodes or other materials prepared by the ECAM method. In addition, the parameters of ECAM itself have been optimised and improved, i.e. the ITO is selected as substrate, and the successful formulation of gel precursors has greatly simplified the process and operational complexity of ECAM. The combination of $Cu(NO_3)_2$ and MC has good compatibility to each other and GO.

Additionally, the samples, Pure Cu and Cu/GO composites with different GO contents, were characterised by SEM for surface morphology observations and Raman and XPS spectroscopy. It was clarified that as the GO content in the precursors increased from 0.1 to 3.0 $wt.\%$ of Cu ions, the GO content on the surface of the deposits increased accordingly.

In terms of corrosion resistance, the GO-added deposits reduced the corrosion current density by anywhere from 26.6% to 65.6% compared to the control group without GO.

6
Future Work

The outlook for future work is in a number of areas. This is because the formation and maintenance of the gel electrolyte meniscus is influenced by many factors including, but not limited to, nozzle size, nozzle travel speed, thermodynamic properties of the electrolyte, thickener concentration, additive composition, ambient humidity, deposition rate and cathode surface wettability to name a few.
First of all, starting from the materials and electrochemical aspects in which we specialise, it is possible to study the concentration of thickeners and the effect of additives on precursors mechanistically (e.g. ionic conductivity tests) and to optimise electrolyte formulations in this way.
In addition, the movement speed of the printing head and the temperature and humidity control of the printing environment can also be developed and adjusted through an engineering approach, in conjunction with part of the production engineering thinking. More importantly, there is currently a considerable lack of control over the size and detail of the printed pattern, and a combination of science and engineering can help us to address this more directly and effectively.
Adequate means of characterisation of the acquired material is naturally of primary importance, and only a more comprehensive characterisation will lead to a deeper knowledge of the material's behaviour. In the future, internal GO distribution and content testing of samples can be investigated by cross-sectional observations and electrical and thermal conductivity tests. Also missing in this paper are mechanical property tests, tensile, bending and compression tests, which are important in relation to the suitability of the material for specific application scenarios.
Although the GO was verified that it does help to the anti-corrosion ability of deposits but the relation between the content of GO and the effects were not sufficiently or clearly proved. It happens due to several uncontrollable variables showed up. Hence, this problem should be carefully considered in future.
In terms of prospects, faster printing speeds and true 3D structures are expected, while maintaining the low cost of operation, because only on this basis can microscale ECAM truly fill the technological gap between conventional metal AM and emerging nano-ECAM and reach the goal of extending the application scenario.

Bibliography

[1] International Organization for Standardization. *Additive manufacturing — General principles — Fundamentals and vocabulary.* ISO/ASTM 52900:2021(en). Vernier, Geneva, Switzerland: International Organization for Standardization, 2021.

[2] Ming Li, Wenchao Du, Alaa Elwany, Zhijian Pei, and Chao Ma. "Metal binder jetting additive manufacturing: a literature review". In: *Journal of Manufacturing Science and Engineering* 142.9 (2020).

[3] William E Frazier. "Metal additive manufacturing: a review". In: *Journal of Materials Engineering and performance* 23 (2014), pp. 1917–1928.

[4] D Hickman, I Ashcroft, S Sharma, X Wang, B Szost, D Johns, AT Clare, et al. "Oxide and spatter powder formation during laser powder bed fusion of Hastelloy X". In: *Powder technology* 354 (2019), pp. 333–337.

[5] Amritbir Singh and Harpreet Singh. "Metal additive manufacturing: from history to applications". In: *Innovations in Additive Manufacturing*. Springer, 2022, pp. 3–32.

[6] Dirk Herzog, Vanessa Seyda, Eric Wycisk, and Claus Emmelmann. "Additive manufacturing of metals". In: *Acta Materialia* 117 (2016), pp. 371–392.

[7] Zhiyuan Liu, Dandan Zhao, Pei Wang, Ming Yan, Can Yang, Zhangwei Chen, Jian Lu, and Zhaoping Lu. "Additive manufacturing of metals: Microstructure evolution and multistage control". In: *Journal of Materials Science & Technology* 100 (2022), pp. 224–236.

[8] John J Lewandowski and Mohsen Seifi. "Metal additive manufacturing: a review of mechanical properties". In: *Annual review of materials research* 46 (2016), pp. 151–186.

[9] Yusheng Shi, Chunze Yan, Yan Zhou, Jiamin Wu, Yan Wang, Shengfu Yu, and Chen Ying. *Materials for Additive Manufacturing*. Academic Press, 2021.

[10] Xinchao Li, Pingmei Ming, Sansan Ao, and Wei Wang. "Review of additive electrochemical micro-manufacturing technology". In: *International Journal of Machine Tools and Manufacture* 173 (2022), p. 103848.

[11] Young-kuk Kim, Donghwa Kang, Hyung-rae Kim, Sung-bin Kim, and Bongyoung Yoo. "The Characteristics of Selective 3D Metal Additive Process Using Electrochemical Deposition and Nozzle Fluid Dynamics". In: *Frontiers in Mechanical Engineering* 6 (2020), p. 9.

[12] JD Whitaker, JB Nelson, and DT Schwartz. "Electrochemical printing: software reconfigurable electrochemical microfabrication". In: *Journal of Micromechanics and Microengineering* 15.8 (2005), p. 1498.

[13] VM Volgin, VV Lyubimov, IV Gnidina, AD Davydov, and TB Kabanova. "Simulation of localized electrodeposition of microwires and microtubes". In: *Procedia CIRP* 68 (2018), pp. 242–247.

[14] Seyedreza Morsali, Soheil Daryadel, Zhong Zhou, Ali Behroozfar, Mahmoud Baniasadi, Salvador Moreno, Dong Qian, and Majid Minary-Jolandan. "Multi-physics simulation of metal printing at micro/nanoscale using meniscus-confined electrodeposition: Effect of nozzle speed and diameter". In: *Journal of Applied Physics* 121.21 (2017), p. 214305.

[15] Aamir Razaq, Faiza Bibi, Xiaoxiao Zheng, Raffaello Papadakis, Syed Hassan Mujtaba Jafri, and Hu Li. "Review on graphene-, graphene oxide-, reduced graphene oxide-based flexible composites: From fabrication to applications". In: *Materials* 15.3 (2022), p. 1012.

[16] Abdulrahman Abu-Nada, Gordon McKay, and Ahmed Abdala. "Recent advances in applications of hybrid graphene materials for metals removal from wastewater". In: *Nanomaterials* 10.3 (2020), p. 595.

[17] Sekhar C Ray. "Application and uses of graphene oxide and reduced graphene oxide". In: *Applications of graphene and graphene-oxide based nanomaterials* 6.8 (2015), pp. 39–55.

[18] Paloma Hidalgo-Manrique, Xianzhang Lei, Ruoyu Xu, Mingyu Zhou, Ian A Kinloch, and Robert J Young. "Copper/graphene composites: a review". In: *Journal of materials science* 54 (2019), pp. 12236–12289.

[19] Ahmed Raslan, Laura Saenz Del Burgo, Jesus Ciriza, and Jose Luis Pedraz. "Graphene oxide and reduced graphene oxide-based scaffolds in regenerative medicine". In: *International Journal of Pharmaceutics* 580 (2020), p. 119226.

[20] Qi Jiang, Peilei Zhang, Zhishui Yu, Haichuan Shi, Di Wu, Hua Yan, Xin Ye, Qinghua Lu, and Yingtao Tian. "A review on additive manufacturing of pure copper". In: *Coatings* 11.6 (2021), p. 740.

[21] Mengze Li, Yang Yang, Francesca Iacopi, Minoru Yamada, and Jaim Nulman. "Compact multilayer bandpass filter using low-temperature additively manufacturing solution". In: *IEEE Transactions on Electron Devices* 68.7 (2021), pp. 3163–3169.

[22] Jakub Marchewka, Ewa Kołodziejczyk, Patryk Bezkosty, and Maciej Sitarz. "Characterization of electrochemical deposition of copper and copper (I) oxide on the carbon nanotubes coated stainless steel substrates". In: *Scientific Reports* 13.1 (2023), p. 6786.

[23] YY Sun, Stefan Gulizia, Darren Fraser, CH Oh, SL Lu, and Ma Qian. "Layer additive production or manufacturing of thick sections of Ti-6Al-4V by selective electron beam melting (SEBM)". In: *Jom* 69 (2017), pp. 1836–1843.

[24] Simon P Stier and Holger Böse. "Electroplating and Ablative Laser Structuring of Elastomer Composites for Stretchable Multi-Layer and Multi-Material Electronic and Sensor Systems". In: *Micromachines* 12.3 (2021), p. 255.

[25] Chenhuinan Wei, Guoxing Wu, Sanjun Yang, and Qiming Liu. "Electrochemical deposition of layered copper thin films based on the diffusion limited aggregation". In: *Scientific Reports* 6.1 (2016), p. 34779.

[26] Joseph R Davis et al. *Copper and copper alloys*. ASM international, 2001.

[27] Jaewon Hwang, Taeshik Yoon, Sung Hwan Jin, Jinsup Lee, Taek-Soo Kim, Soon Hyung Hong, and Seokwoo Jeon. "Enhanced mechanical properties of graphene/copper nanocomposites using a molecular-level mixing process". In: *Advanced materials* 25.46 (2013), pp. 6724–6729.

[28] Chokkakula LP Pavithra, Bulusu V Sarada, Koteswararao V Rajulapati, Tata N Rao, and G Sundararajan. "A new electrochemical approach for the synthesis of copper-graphene nanocomposite foils with high hardness". In: *Scientific reports* 4.1 (2014), p. 4049.

[29] Meixia Li, Hongwei Che, Xiaoyan Liu, Shunxing Liang, and Hailong Xie. "Highly enhanced mechanical properties in Cu matrix composites reinforced with graphene decorated metallic nanoparticles". In: *Journal of materials science* 49 (2014), pp. 3725–3731.

[30] Ding-Bang Xiong, Mu Cao, Qiang Guo, Zhanqiu Tan, Genlian Fan, Zhiqiang Li, and Di Zhang. "High content reduced graphene oxide reinforced copper with a bioinspired nano-laminated structure and large recoverable deformation ability". In: *Scientific reports* 6.1 (2016), p. 33801.

[31] Youbin Kim et al. "Strengthening effect of single-atomic-layer graphene in metal–graphene nanolayered composites". In: *Nature communications* 4.1 (2013), p. 2114.

[32] Ding-Bang Xiong, Mu Cao, Qiang Guo, Zhanqiu Tan, Genlian Fan, Zhiqiang Li, and Di Zhang. "Graphene-and-copper artificial nacre fabricated by a preform impregnation process: bioinspired strategy for strengthening-toughening of metal matrix composite". In: *Acs Nano* 9.7 (2015), pp. 6934–6943.

[33] Ewald Heitz. "Corrosion of metals in organic solvents". In: *Advances in Corrosion Science and Technology: Volume 4* (1974), pp. 149–243.

[34] Nasser Kanani. *Electroplating: basic principles, processes and practice*. Elsevier, 2004.

[35] Allen J Bard, Larry R Faulkner, and Henry S White. *Electrochemical methods: fundamentals and applications*. John Wiley & Sons, 2022.

[36] Xiaolong Chen, Xinhua Liu, Mengzheng Ouyang, Jingyi Chen, Oluwadamilola Taiwo, Yuhua Xia, Peter Childs, Nigel P Brandon, and Billy Wu. "Multi-metal 4D printing with a desktop electrochemical 3D printer". In: *Scientific reports* 9.1 (2019), pp. 1–9.

[37] J Brady, Thomas Dürig, PI Lee, and J-X Li. "Polymer properties and characterization". In: *Developing solid oral dosage forms*. Elsevier, 2017, pp. 181–223.

[38] Pauline L Nasatto, Frédéric Pignon, Joana LM Silveira, Maria Eugênia R Duarte, Miguel D Noseda, and Marguerite Rinaudo. "Methylcellulose, a cellulose derivative with original physical properties and extended applications". In: *Polymers* 7.5 (2015), pp. 777–803.

[39] Soheil Daryadel, Ali Behroozfar, S Reza Morsali, Salvador Moreno, Mahmoud Baniasadi, Julia Bykova, Rodrigo A Bernal, and Majid Minary-Jolandan. "Localized pulsed electrodeposition process for three-dimensional printing of nanotwinned metallic nanostructures". In: *Nano letters* 18.1 (2018), pp. 208–214.

[40] Jae Young Park and Seok Kim. “Preparation and electroactivity of polymer-functionalized graphene oxide-supported platinum nanoparticles catalysts”. In: *International journal of hydrogen energy* 38.14 (2013), pp. 6275–6282.

[41] Juan Yang, Xingbin Yan, Jiangtao Chen, Haibin Ma, Dongfei Sun, and Qunji Xue. “Comparison between metal ion and polyelectrolyte functionalization for electrophoretic deposition of graphene nanosheet films”. In: *RSC advances* 2.25 (2012), pp. 9665–9670.

[42] Anshul Kamboj, Y Raghupathy, MY Rekha, and Chandan Srivastava. “Morphology, texture and corrosion behavior of nanocrystalline copper–graphene composite coatings”. In: *Jom* 69.7 (2017), pp. 1149–1154.

[43] Wafaa M Hosny, Afkar K Abdel Hadi, Houssni El-Saied, and Altaf H Basta. “Metal chelates with some cellulose derivatives. Part III. Synthesis and structural chemistry of nickel (II) and copper (II) complexes with carboxymethyl cellulose”. In: *Polymer international* 37.2 (1995), pp. 93–96.

[44] Takashi Kobayashi, Makoto Yoshimoto, and Katsumi Nakao. “Preparation and characterization of immobilized chelate extractant in PVA gel beads for an efficient recovery of copper (II) in aqueous solution”. In: *Industrial & engineering chemistry research* 49.22 (2010), pp. 11652–11660.

[45] DR Sparks and GM Vest. “Copper films from aqueous solutions of copper nitrate trihydrate”. In: *Thin solid films* 200.1 (1991), pp. 77–82.

[46] Artorn Pokaipisit, Mati Horprathum, and Pichet Limsuwan. “Effect of films thickness on the properties of ITO thin films prepared by electron beam evaporation”. In: *Agriculture and Natural Resources* 41.5 (2007), pp. 255–261.

[47] Dongmok Lee, Gi Duk Kwon, Jung Ho Kim, Eric Moyen, Young Hee Lee, Seunghyun Baik, and Didier Pribat. “Significant enhancement of the electrical transport properties of graphene films by controlling the surface roughness of Cu foils before and during chemical vapor deposition”. In: *Nanoscale* 6.21 (2014), pp. 12943–12951.

[48] V Brusic, GS Frankel, J Roldan, and Ravi Saraf. “Corrosion and protection of a conductive silver paste”. In: *Journal of the Electrochemical Society* 142.8 (1995), p. 2591.

[49] Goki Eda and Manish Chhowalla. “Chemically derived graphene oxide: towards large-area thin-film electronics and optoelectronics”. In: *Advanced materials* 22.22 (2010), pp. 2392–2415.

[50] Ji Chen, Bowen Yao, Chun Li, and Gaoquan Shi. “An improved Hummers method for eco-friendly synthesis of graphene oxide”. In: *Carbon* 64 (2013), pp. 225–229.

[51] Yakun Chen, Xiang Zhang, Enzuo Liu, Chunnian He, Chunsheng Shi, Jiajun Li, Philip Nash, and Naiqin Zhao. “Fabrication of in-situ grown graphene reinforced Cu matrix composites”. In: *Scientific reports* 6.1 (2016), p. 19363.

[52] Ori Geuli and Daniel Mandler. “The synergistic effect of benzotriazole and trimethylsiloxysilicate towards corrosion protection of printed Cu-based electronics”. In: *Corrosion Science* 143 (2018), pp. 329–336.

[53] H Otmačić, J Telegdi, K Papp, and E Stupnišek-Lisac. “Protective properties of an inhibitor layer formed on copper in neutral chloride solution”. In: *Journal of Applied Electrochemistry* 34 (2004), pp. 545–550.

[54] Y Raghupathy, Anshul Kamboj, MY Rekha, NP Narasimha Rao, and Chandan Srivastava. “Copper-graphene oxide composite coatings for corrosion protection of mild steel in 3.5% NaCl”. In: *Thin Solid Films* 636 (2017), pp. 107–115.

[55] Jiang Yang, Shengyuan Deng, Jianping Lei, Huangxian Ju, and Sundaram Gunasekaran. “Electrochemical synthesis of reduced graphene sheet–AuPd alloy nanoparticle composites for enzymatic biosensing”. In: *Biosensors and Bioelectronics* 29.1 (2011), pp. 159–166.

[56] J Gravier, V Vignal, and S Bissey-Breton. “Influence of residual stress, surface roughness and crystallographic texture induced by machining on the corrosion behaviour of copper in salt-fog atmosphere”. In: *Corrosion Science* 61 (2012), pp. 162–170.

A

Source G-code listing

```
M73 P0; enable build progress
G21; set units to mm
G90; set positioning to absolute
G162 X Y F3000; home XY axes maximum
G161 Z F450; home Z axis minimum
G92 X0 Y0 Z0 E0
G92 X150 Y90 Z0 E0
M132 Z; Recall stored home offset for Z axis
G1 X0 Y115 Z0 F3000; change this Z to change print hight
M420 R1 E8 B85 P0
G92 E0 ; Set E to 0
; process Process for X/Y movement test
; layer 1, Z = 0.001
M135 T0
G1 E-2.3000 F1800
; feature outer perimeter
; tool H0.001 W0.250
G1 Z0.001 F600
G1 X3.873 Y44.975 F12000
G1 E2.3000 F1800
G1 X3.873 Y45.025 E0.0000 F9
G1 X-3.875 Y45.025 E0.0003
G1 X-3.875 Y44.975 E0.0000
G1 X3.873 Y44.975 E0.0003
; layer 2
G1 Z0.002 F600
G1 X3.875 Y45.025 E0.0000 F30
G1 X-3.875 Y45.025 E0.0003
G1 X-3.875 Y44.975 E0.0000
G1 X3.875 Y44.975 E0.0003
M73 P100 ; end build progress
G91
G1 X0 Y0 Z150 F1000 ; send Z axis to bottom of machine
G90
G162 X Y F3000 ; home XY maximum
M70 P5 ; Print Finished
```

B

Initial project

Before this thesis work, few primarily works were done for establishing the prototype of ECAM process. Different 3D models was tested and optimised based on the feature of ECAM deposits, and both substrates and the type and size of nozzle was investigated for better printing resolution. Eventually, pure Cu on Cu foil was successfully performed with a minimum feature size of 400 μm, approximately.

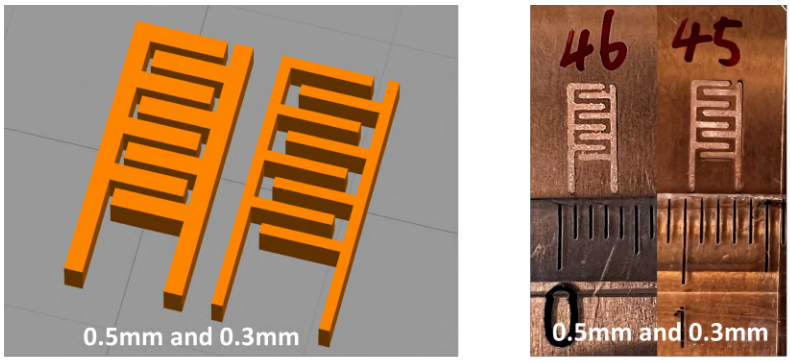

Figure B.1: Optimisation of 3D models.

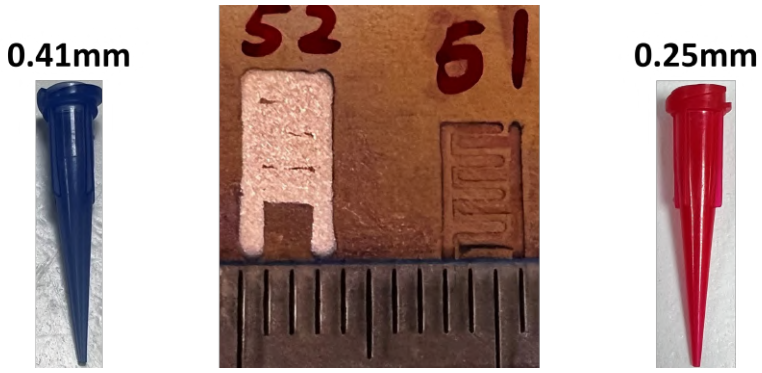

Figure B.2: Optimisation of nozzle size.

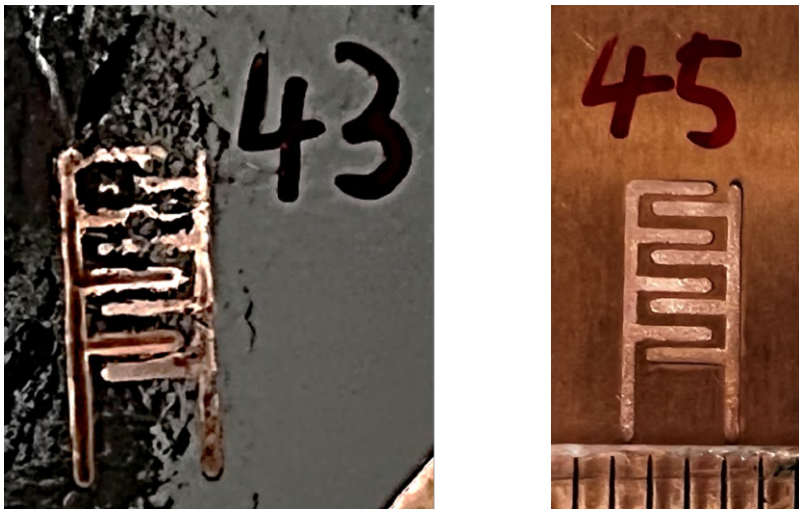

Figure B.3: Optimisation of substrate selection.

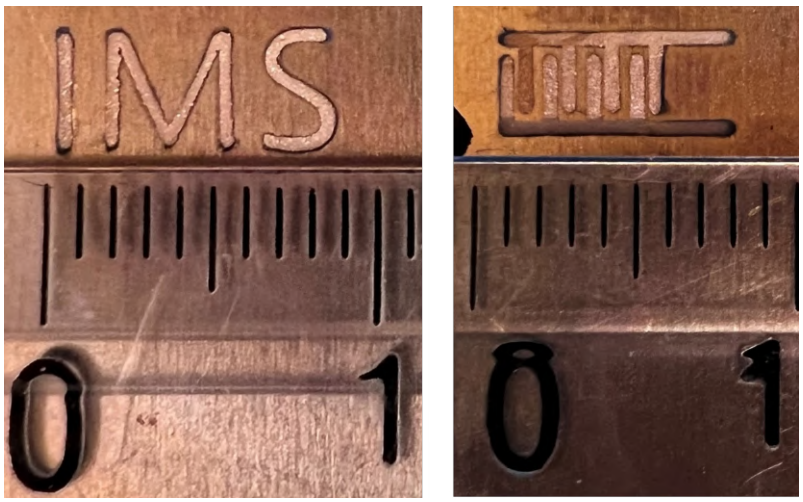

Figure B.4: Arbitrarily shaped and interlaced electrodes on Cu foil.

With this project, the basic procedure was laid down and the main questions could be defined.

DEPARTMENT OF INDUSTRIAL AND MATERIALS SCIENCE
CHALMERS UNIVERSITY OF TECHNOLOGY
Gothenburg, Sweden
www.chalmers.se

CHALMERS
UNIVERSITY OF TECHNOLOGY